CHALMERS
UNIVERSITY OF TECHNOLOGY

Implementation of Active Noise Control on the air intake of a truck

Master's Thesis in the Master Degree program, Sound and Vibration

Alexander Henriksson
Örn Smári Blumenstein

Department of Architecture and Civil Engineering, Division of Applied Acoustics
CHALMERS UNIVERSITY OF TECHNOLOGY
Gothenburg, Sweden 2018

Master's thesis 2018:BOMX02-18-3

Implementation of Active Noise Control on the air intake of a truck

Alexander Henriksson
Örn Smári Blumenstein

CHALMERS
UNIVERSITY OF TECHNOLOGY

Department of Architecture and Civil Engineering, Division of Applied Acoustics
Chalmers University of Technology
Gothenburg, Sweden 2018

Implementation of Active Noise Control on the air intake of a truck
Alexander Henriksson
Örn Smári Blumenstein

Supervisors: Frédéric Wullens, Cross Spectrum
Tor Möller, Noise and vibration laboratory at Volvo trucks
Examiner: Wolfgang Kropp, Division of Applied Acoustics University

Master's Thesis 2018:BOMX02-18-3
Department of Architecture and Civil Engineering, Division of Applied Acoustics
Chalmers University of Technology
SE-412 96 Gothenburg
Telephone +46-(0)31-772 2200

Typeset in LaTeX

Implementation of Active Noise Control on the air intake of a truck
Alexander Henriksson
Örn Smári Blumenstein
Department of Architecture and Civil Engineering, Division of Applied Acoustics
Chalmers University of Technology

Abstract

Noise control using passive solutions like damping layers, rubber bushings and absorption materials are well established and successful methods, but show limits in the low frequency range. An alternative to passive measures is the implementation of active noise control, first presented by Paul Leg in 1934. Advances in appropriate low latency processing units required for active control over the last years and the possibility of high-level programming have lowered the implementation costs for realizing an active noise control system. On a truck, the air intake system is connected to the rear wall of the cabin and the pressure pulsations inside the intake system produce air borne noise in the cabin from the duct mouth and the duct wall. Structure borne noise is transferred via the connections with the rear wall. The cabin noise is today optimized with passive measures.

This master's thesis is about the feasibility assessment and the implementation of active noise control in the air intake system of a truck to optimize the cabin noise in the frequency range 20 Hz to 350 Hz. To do so, the air intake system from a truck is mounted on a aluminum rig to serve as experimental setup. A single channel feedforward NBFXLMS controller is proposed for the implementation. The controller is implemented using a block-based LMS algorithm making the controller versatile for possible future implementations both in time and frequency domain. Offline and adaptive implementations are compared with measurements and virtual simulations in Simulink. An investigation on the control loudspeaker limitations shows that the loudspeaker used in the project cannot produce the sound pressure levels required in the test conditions due to maximum consumed power and maximum excursion limits. Due to the control loudspeaker limitations, final measurements were carried out at lower sound pressure levels were the control loudspeaker operates within it's operating limits.The results show that an active control system is technically possible to implement.

The obtained reduction for air borne sound at the inlet mouth and structure borne vibrations transmitted to the aluminum rig is up to 15dB for sound pressure and acceleration levels in the frequency range of interest at several truck driving conditions. To be able to control the actual sound pressure levels in the air intake system a new control loudspeaker study is suggested.

Keywords: ANC, active noise control, FXLMS, NBFXLMS, air intake, adaptive.

Acknowledgements

We would like to thank our supervisors Wolfgang Kropp, Frédéric Wullens and Tor Möller for their help and support writing this thesis. We would also like to thank Sophie Girolami for providing pressure maps of the air intake and all the personal at the noise and vibration laboratory at Volvo trucks and the division of Applied Acoustics at Chalmers university for their help and support.

Gothenburg, Mars 2018
Alexander Henriksson
Örn Smári Blumenstein

Contents

List of Figures

List of Tables

1

Introduction

The cabin of a truck is a work place and drivers spend several hours at one stretch inside the cabin [1]. Today the A-weighted sound pressure level in trucks are low enough not to be harmful [2]. There is no immediate reason to reduce the sound pressure levels further,but the need to be able to improve the overall impression of the truck is still desirable to be able to keep a high standard of interior sound quality inside the cabin. Sound quality is a mix of low or nonexistent noise levels from truck components that the driver does not need acoustic feedback from, and of well balanced and designed functional noise that helps the driver in his work. Examples of functional noise for instance are the sound of the engine and the sound of the activated engine brake. A schematic drawing of the air intake system is shown in Figure 1.1.

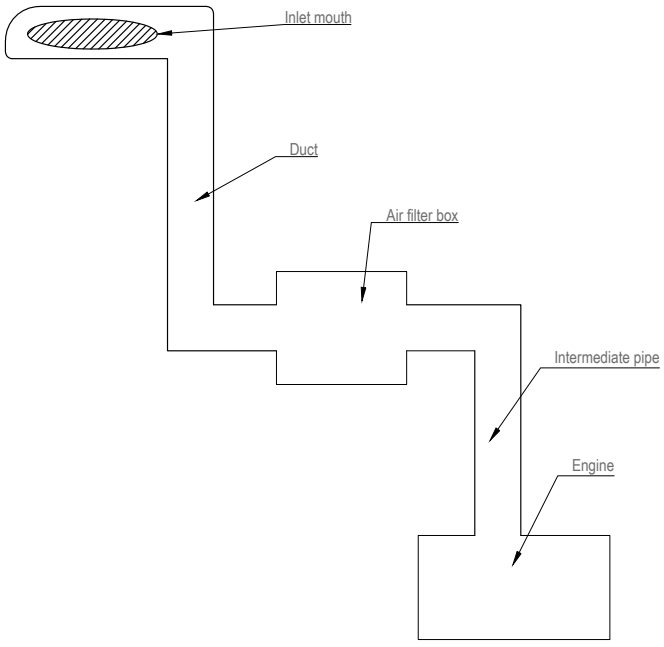

Figure 1.1: Schematic drawing of the air intake.

Assuming that the air intake system of a truck is elastic, a time varying internal

pressure inside the duct will force the duct walls of the to vibrate, the vibrations will cause the duct to start radiating noise to the back of the cabin, through the cabin rear wall, into the cabin. The duct is fastened to the cabin wall with rubber bushings and vibrations transferred from the inlet system to the bushings will excite the cabin wall and cause it to radiate noise into the cabin. The inlet mouth is located on the top of the cabin, pressure fluctuations inside the duct will cause an vibrating air column to radiate noise at the inlet mouth into the cabin through the walls and windows. If the pressure level inside the air intake system is lowered the noise level inside the truck-cabin could be lowered.

This project is done in cooperation with Volvo Trucks with the aim to investigate if it is technically possible to increase the insulation between a air intake system and a cabin on a truck by using active noise control(ANC) on the trucks air intake system. The project is limited to single channel control system controlling plane waves which limits the frequency range of the controller. The control loudspeaker provides a limitation in achievable sound pressure levels to be controlled.

2

Theory

2.1 Introduction to Active Noise Control

Passive approaches have traditionally been used to control sound pressure levels in different sound fields. Passive approaches are suitable for absorbing mid and high range frequencies but are expensive and impractical for controlling lower frequencies due to the long wave lengths involved.

Active noise control strategies for controlling low frequency noise in a duct can be implemented using one or several loudspeakers in an duct to achieve:

- Local control
- Global control
- Minimize radiated sound power
- Active impedance control

All of the above strategies can be implemented and designed using either a feed-forward or a feedback system controller, see Figure 2.1. In feed-forward control the wavefront is measured at the reference sensor processed and sent forward to the control loudspeaker. In feedback control the wavefront is measured past the control loudspeaker and then fed back to the control system. If a good reference signal can be obtained feed-forward control is in general considered to be superior to a feedback system. [3].

In this thesis a local feed-forward controller will be investigated. The purpose of the control system is to control the sound field inside a duct close to and around the position of the error microphone. The system must respond to the wave front with a calculated destructive wave front in the duct before it passes by the control loudspeaker location in the inlet system to cancel the disturbance.

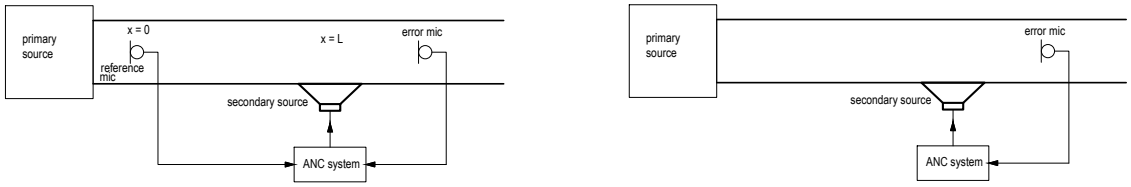

(a) Feed-forward controller.

(b) Feedback controller.

Figure 2.1: Feed-forward and feedback controller structure.

Local sound cancellation of low frequency sound in a duct is accomplished using the principle of wave superposition [4]. If the sound in the duct is constant over the whole cross-section of the duct, exception is the area around the control loudspeaker and very close to the walls of the duct, the sound waves are said to be plane waves. Plane waves in a duct appear at low frequencies as long as no cross modes have been excited in the duct. The cut-off frequency for plane wave propagation in a duct can be approximated with equation 2.1, the wave length of the noise needs to be approximately six times bigger then the diameter of the tube [5].

$$f_{cut-off} = \frac{c_o}{6d_{tube}}, \tag{2.1}$$

Cancellation of plane waves in a duct generated by a source, with a source strength q_p can be accomplished using a single control loudspeaker with source strength q_s. If more complicated sound fields are present a multiple loudspeaker approach is required [4].

A two dimensional sound field created in a duct with two ideal sound sources can be calculated with equations 2.2 and 2.3. Both sound sources are assumed to be mounted on a infinite baffle generating plane waves only in a duct with a constant cross section S. The primary sound source is located at position $x = 0$ and the secondary sound source is located at $x = L$. The sound pressure and density in the enclosure are assumed to be small compared to their ambient values and the particle velocity is assumed to be much lower than the speed of sound c_0 [4].

$$\begin{aligned} p_{primary}(x) &= \tfrac{q_p}{2S}\rho_0 c_0 e^{-jkx} e^{j\omega t}, x > 0 \\ p_{primary}(x) &= \tfrac{q_p}{2S}\rho_0 c_0 e^{jkx} e^{j\omega t}, x < 0 \end{aligned} \tag{2.2}$$

$$\begin{aligned} p_{secondary}(x) &= \tfrac{q_p}{2S}\rho_0 c_0 e^{-jk(x-L)}, x > L \\ p_{secondary}(x) &= \tfrac{q_p}{2S}\rho_0 c_0 e^{jk(x-L)}, x < L \end{aligned} \tag{2.3}$$

Having the objective to cancel the sound pressure down the duct past the location $x > L$ in the duct the equations for the total sound pressure can be rewritten as a super position of the two waves fronts in the duct:

$$P_{x>L} = \frac{\rho_0 c_0}{2S}\left(q_p e^{-jkx} + q_s e^{-jkx} e^{jkL}\right) = 0 \tag{2.4}$$

The control loudspeaker in the duct could be used to cancel the sound pressure generated by the primary source if the source strength of the control loudspeaker is an exact copy of the primary noise with opposite phase and an frequency depending phase shift according to equation 2.5 [6].

$$q_s = -q_p e^{-jkL} \tag{2.5}$$

Equation 2.5 is also called the feed forward control law and is the centre of feed forward active noise control systems.

2.1.1 Single channel feed forward control in a duct

A single channel feed-forward controller can be implemented in either adaptive(online) or non adaptive(offline) mode. In Figure 2.2 a block diagram for a offline feed-forward control system in the frequency domain is shown. $P(j\omega)$ is the frequency response of the primary path and is defined as

$$P(j\omega) = \left.\frac{E(\omega)}{X(\omega)}\right|_{S(\omega)=0} \tag{2.6}$$

with the secondary source turned off so that $S(\omega) = 0$. The output is then $E(\omega)$, the frequency response at the error sensor and reference input is $X(\omega)$, the frequency response at the reference sensor. The secondary path is the path from the reference sensor trough the electronic control system, control loudspeaker and the physical path between the control loudspeaker and the error microphone lumped together. The frequency response of the secondary path, $C(j\omega)$, is defined as

$$C(j\omega) = \left.\frac{E(\omega)}{Y(\omega)}\right|_{D(\omega)=0} \tag{2.7}$$

with the primary source turned off so that $D(\omega) = 0$. The output is the error sensor signal $E(\omega$ and the reference input is $Y(\omega)$, the control filter signal. Finally $H(j\omega)$ is the control filter.

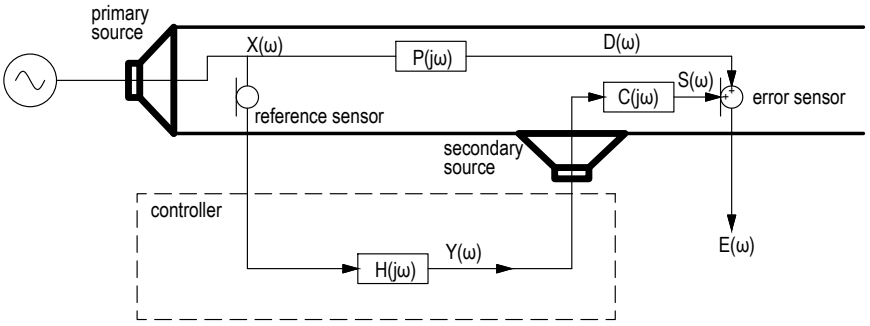

Figure 2.2: Block diagram for controlling sound in a duct in frequency domain.

To drive the error $E(\omega)$ to zero the control law to cancel the noise past the location of the error microphone for the controller $H(j\omega)$ can be calculated, assuming there is no feedback from the control loudspeaker to the microphone or measurement noise, to be:

$$H(j\omega) = -\frac{P(j\omega)}{C(j\omega)} \tag{2.8}$$

2.2 Least mean-square algorithm

A adaptive filter can be described as a filter that will adjust its coefficients to reduce the error so that the output of the filter matches a desired output. The error is formed by subtracting a desired output from the filtered output. Figure 2.3 shows a block diagram of a typical adaptive filtering problem [7].

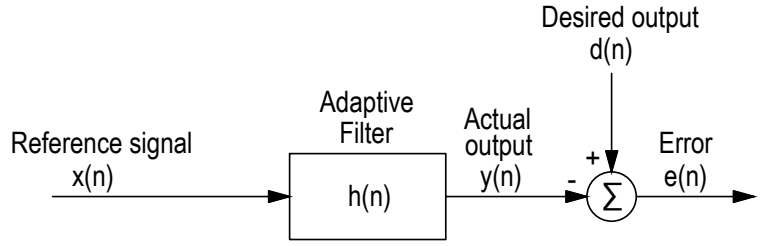

Figure 2.3: Block diagram showing a standard adaptive filtering problem.

A common way to solve the adaptive filtering problem is to adjust the filter coefficients so that the mean square error is minimized, By differentiating the instantaneous error with respect to the filter coefficients the LMS uses a estimate of the gradient rather than the true gradient. The least mean square algorithm(LMS) is the most commonly used algorithm for adjusting the coefficients in a adaptive

linear filter. The LMS is heavily used in active control due to its simplicity in implementation and calculations [7]. A implementation of the LMS can be described as following [3]. At each iteration, n, a new FIR filter output is calculated as

$$y(n) = \mathbf{x}(n)^T \mathbf{h}(n) \tag{2.9}$$

were $\mathbf{h}(\mathbf{n})$ is a FIR filter with N coefficients

$$\mathbf{h}(n) = [h_0(n) \quad h_1(n) \cdots h_{N-1}(n)]^T \tag{2.10}$$

and $\mathbf{x}(\mathbf{n})$ is the current and past N values of the reference signal

$$\mathbf{x}(n) = [x(n) \quad x(n-1) \cdots x(n-(N-1))]^T \tag{2.11}$$

The error is the difference between the desired output and the actual output and is obtained as

$$e(n) = d(n) - y(n) \tag{2.12}$$

The filter is then updated using the error function $e(n)$, reference signal $\mathbf{x}(n)$ and the convergence factor μ.

$$\boldsymbol{h}(n+1) = \boldsymbol{h}(n) + 2\mu \boldsymbol{x}(n) e(n) \tag{2.13}$$

The rate of convergence is dependant on the convergence coefficient also called step size, μ. The step size affects the obtainable mean square error and will determine the convergence rate of the algorithm. The step size determines the ratio of how much the actual error and in-signal(reference) affect the update of the filter coefficients. A small step size value will result in slow converge and large step size value results in fast convergence. Too large step size value will result in divergence of the algorithm [8]. To improve the convergence rate a variable step size or normalisation of the reference signal can be used. In the normalised LMS the filter update equation becomes

$$\boldsymbol{h}(k+1) = \boldsymbol{h}(k) + \frac{\mu_n}{\gamma + \boldsymbol{x}^T(k)\boldsymbol{x}(k)} e(k)\boldsymbol{x}(k) \tag{2.14}$$

were μ_n is a fixed convergenge factor with value $0 < \mu_n \leq 1$, γ is a small constant added to avoid large step sizes when $\boldsymbol{x}^T(k)\boldsymbol{x}(k)$ becomes small [9].

2.2.1 Inverse filtering

The LMS algorithm can be used to obtain an stable inverse filter of a system in an optimal way. This can be used for example to equalize the room gain on a recorded signal.

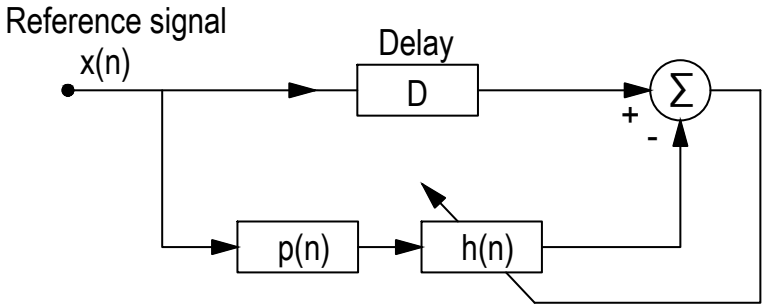

Figure 2.4: Block diagram showing inverse filtering.

A block diagram to obtain an inverse filter, $\mathbf{h}(n)$, for a system represented with the impulse response function $\mathbf{p}(n)$ using the LMS algorithm is shown in Figure 2.4. To obtain a inverse filter the reference signal to the LMS is filtered with an estimation of the system to obtain an inverse for. The delay, D, seen in Figure 2.4 is not necessary but will make the obtained inverse filter stable whether the system to obtain an inverse for is minimum phase or not. To check if the inverse function is truly a inverse, convoluting the impulse response function $\mathbf{p}(n)$ and the estimated inverse impulse response function, $\mathbf{h}(n)$, should result in a delayed unit impulse in the time domain.

2.2.2 System identification

The LMS algorithm can also be used in modeling or identification of an unknown dynamic system. A block diagram to model a unknown system represented with the impulse response, $\mathbf{p}(n)$, using the LMS algorithm is shown in Figure 2.5.

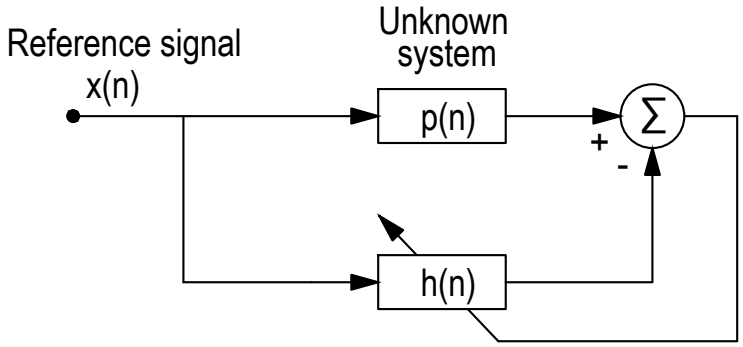

Figure 2.5: Block diagram showing system identification.

2.2.3 Filtered-x LMS(FxLMS)

The FxLMS is a widely adopted type of LMS-algorithm used for feed-forward controllers in active control. The FxLMS filter can be implemented in both offline and online mode. General properties of the FxLMS algorithm is that it is a robust algorithm and relatively fast. It is robust to error in the estimated secondary paths phase response up to 90°. In the FxLMS the reference signal, x, is filtered with a finite impulse response estimate of the secondary path before the filter update is carried out, therefore the name Filtered-x. This is done to compensate for the existence of the secondary path [4].

2.2.3.1 Offline FxLMS

The control filter $\mathbf{h}(n)$ is calculated before being uploaded to the controller with a training signal and known impulse responses for the primary path and the secondary path, $\hat{\mathbf{p}}(n)$ and $\hat{\mathbf{c}}(n)$ using the block diagram in Figure 2.6. In the block diagram for calculating the optimal filter the measured secondary path is moved in front of the controller to obtain the filtered reference signal, this shift of transfer functions blocks is allowed if the transfer functions are assumed to be linear and time invariant [4].

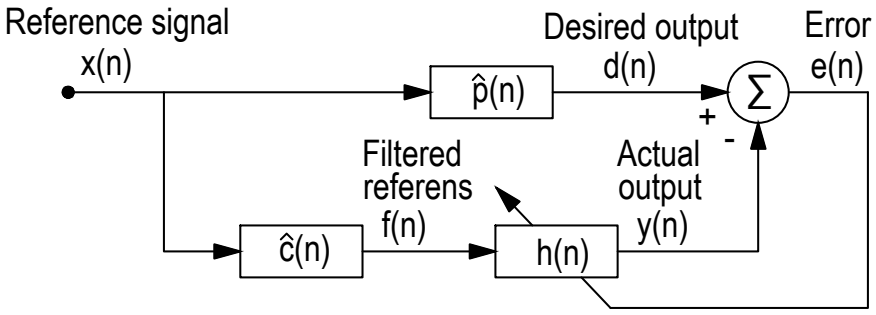

Figure 2.6: Offline controller calculations.

From the block diagram in 2.6 the error becomes

$$e(n) = d(n) - y(n) \tag{2.15}$$

were $d(n)$ is the signal after the reference signal has being convoluted with the finite impulse response of the primary path. $\mathbf{f}(n)$ is the "filtered x", it is the convolution of the reference signal with a finite impulse response of the secondary path. $\mathbf{f}(n) = \mathbf{x}^T(n)\mathbf{c}(n)$. $y(n)$ is the output from the control filter $\mathbf{h}(n)$, $y(n) = \mathbf{f}^T(n)\mathbf{h}(n)$. The filter update can then be written as

$$\mathbf{h}(n+1) = \mathbf{h}(n) + 2\mu\mathbf{f}(n)e(n) \tag{2.16}$$

The control filter obtained using the block diagram in 2.6 has a estimation of the secondary path, $\hat{\mathbf{c}}(n)$, located before the control filter which will return a inverse estimate of $\mathbf{c}(n)$ and a system identification of $\mathbf{p}(n)$. After the filter has converged the filter will be that of the control law in equation 2.8.

2.2.3.2 Online FxLMS

In adaptive or online mode there are some differences in the implementation of the FxLMS from the offline. The control filter $\mathbf{h}(n)$ is then adaptive and the physical impulse responses of the primary path, $\mathbf{p}(n)$, and the secondary path, $\mathbf{c}(n)$, are included in the controller update process. The primary path, $\mathbf{p}(n)$, can be unknown but a estimation of the secondary path, $\mathbf{c}(n)$, needs to be known. In Figure 2.7 the online FxLMS setup is shown. In the online implementation the psychical impulse response $\mathbf{c}(n)$ is a part of the algorithm, located after the control filter. To obtain the control law presented in 2.8 the FxLMS filter update equation needs to have a filtered reference signal, that is the reference signal convoluted with the a estimate of the secondary path, $\hat{\mathbf{c}}(n)$, while the filtering process of the reference signal going trough the control filter, $\mathbf{h}(n)$ and $\mathbf{c}(n)$ is independent of in which order the filtering is done. This is solved by updating the control filter parallel to the filtering process as seen in Figure 2.7.

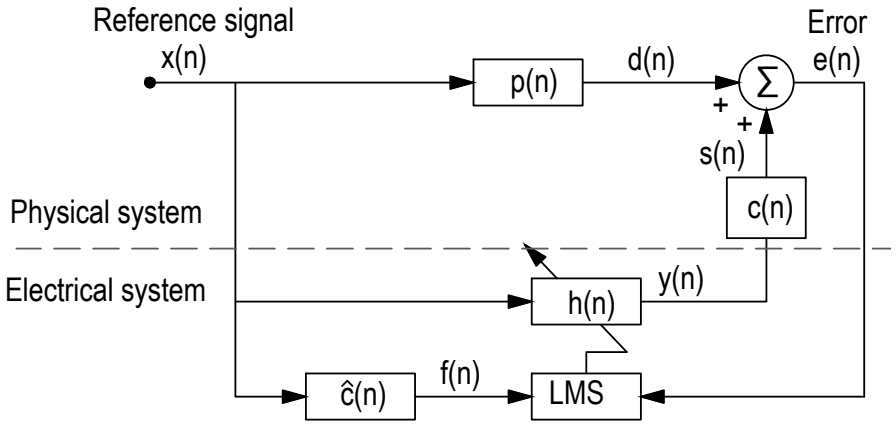

Figure 2.7: Block diagram for FxLMS in online mode.

At each iteration, n the output from the control filter is

$$y(n) = \mathbf{x}^T(n)\mathbf{h}(n) \tag{2.17}$$

The control source output, $s(n)$ is the convolution of the filter output $y(n)$ and the physical secondary path $\mathbf{c}(n)$

$$s(n) = \mathbf{y}^T(n)\mathbf{c}(n) \tag{2.18}$$

Another difference implementing the FxLMS online is that all summation signs become addition, since transducers can only add signals. The signal from the error microphone will now be

$$e(n) = d(n) + s(n) \tag{2.19}$$

were $d(n)$ is the generated disturbance after the source signal has being convoluted with the primary path. Finally the filter update can be written as

$$\boldsymbol{h}(n+1) = \boldsymbol{h}(n) - 2\mu e(n)\boldsymbol{f}(n) \tag{2.20}$$

were $\boldsymbol{f}(n)$ is the filtered reference signal, the reference signal $\mathbf{x}(n)$ convoluted with estimate of the secondary path, $\hat{\mathbf{c}}(n)$.

$$\boldsymbol{f}(n) = \mathbf{x}^T(n)\hat{\mathbf{c}}(n) \tag{2.21}$$

2.2.4 Feedback Neutralization

When a microphone is used as a reference sensor the microphone will pick up the control signal coming from the control loudspeaker. This will introduce a feedback path, $F(j\omega)$, in the system. Figure 2.2 from Section 2.1.1 is now extended to include the feedback path and feedback compensation, see Figure 2.8. The frequency response of the feedback path is modelled as

$$F(j\omega) = \left.\frac{X(j\omega)}{Y(j\omega)}\right|_{R(j\omega)=0} \tag{2.22}$$

were the primary source is turned off making $R(\omega) = 0$. The feedback path has the same reference input as the secondary path, $Y(\omega)$ but the output is the reference microphone signal $X(\omega)$. The feedback path can cause acoustic feedback if the gain is high enough and can deteriorate the reference signal and can cause instability in the control system. There are couple of solutions to this problem. One is to use directional sensors and or directional control sources. Another solution is using signal processing techniques. The feedback path is then estimated and removed from the reference signal within the controller, see Figure 2.8.

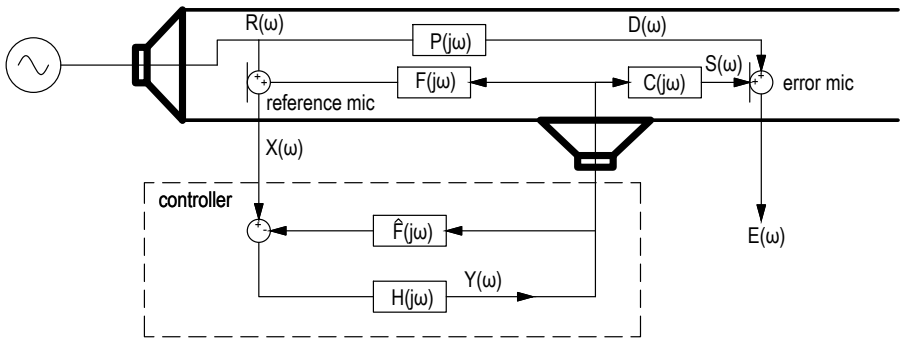

Figure 2.8: Feedback compensation.

If the feedback path, $F(j\omega)$, is modelled accurately so that: $\hat{F}(j\omega) \approx -F(j\omega)$, it is possible to almost neutralize the feedback path. Feedback neutralization by adding a second feedback loop within the controller itself can cause the system to become unstable. The controller can be kept stable using this approach by ensuring the gain of the controller does not exceeds unity gain, upholding the Nyquist stability criterion.

2.2.5 Block based FxLMS

An alternative implementation of the sample by sample FxLMS is an block based version of the algorithm. A block based least mean square schematic extends the

controllers ability to filter signals of infinite lengths in both time and frequency-domains, making it a very good experimental platform to build from. There are mainly two methods used to support block based filtering. These are Overlap-add method and Overlap-save method see Figure 2.9. The method used in this report is the Overlap-save method.

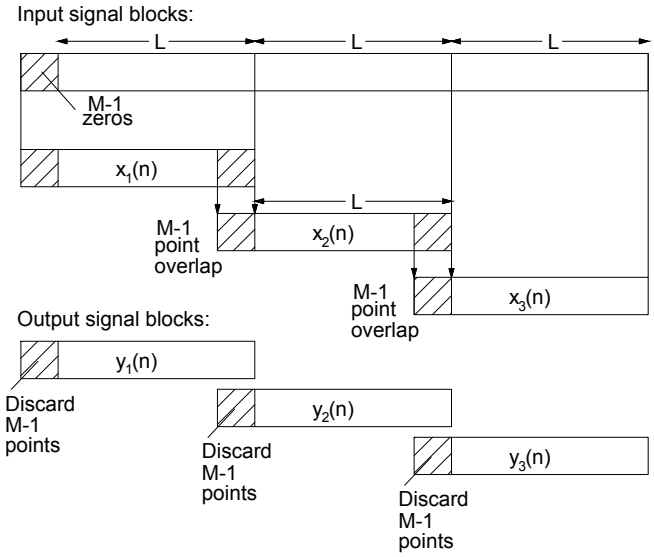

Figure 2.9: Overlap save method

The controllers filter taps are updated after each collected block of data samples. The size of each block, L, should be equal or more than the filter tap length N. Some of the past input samples need to be saved to be able to reuse them when performing the filtering operation on the next block. This is done by using a ”dummy” vector of length M-1 plus the size of the input data block-size. When the function is called it is assumed that the M-1 ”old” samples of the input are stored in the beginning of the state vector. By then also adding the new input data to the same vector we have one long vector which contain all data needed to produce the entire block filtered output.[8]

2.3 Delay

The electrical delay in the secondary path is a limiting factor in the system design since it sets at limit on the distance between the reference microphone and the control loudspeaker. In a feedforward controller causality constrain must be met for random or non-periodic signals. Slowly varying periodic signals dont need to meet this condition since the characteristics of one period are assumed to be sufficiently similar to the period preceding it [3]. In order for the controller to react in time on the signal measured at the reference microphone the time it takes sound to propagate

from the reference microphone location to the error microphone location has to be greater then the electrical delay in the secondary path, see Figure 2.10.

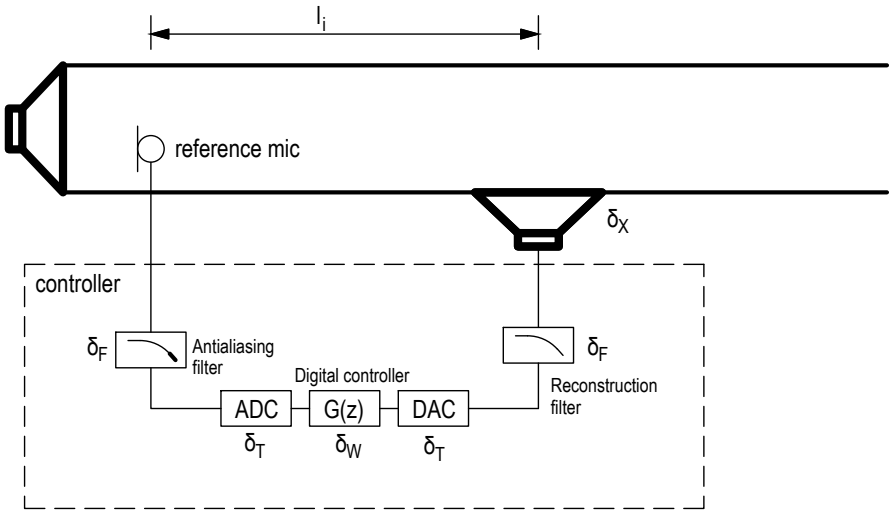

Figure 2.10: Delays in feed-forward controller.

The total electric delay in the secondary path consists of

$$\delta_E = \delta_X + \delta_F + \delta_T + \delta_W \tag{2.23}$$

were δ_X is the delay of the control loudspeaker, δ_F is the delay in the analog anti aliasing and reconstruction filters estimated by

$$\delta_F = n/8f_c \tag{2.24}$$

were n is the filter order and f_c is the cut off frequency [4], δ_T is the delay for AD/DA conversion and one sample processing time and δ_W is the delay of the digital controller. The causality constrain can now be formulated as

$$\delta_A \geq \delta_E \tag{2.25}$$

were δ_E it the total electrical delay in the secondary path and δ_A is the acoustic delay for the time it takes sound to propagate from the reference microphone location to the error microphone location, $\delta_A = l_i/c$, were l_i is the length between reference microphone and the control loudspeaker [10].

It is known that δ_F and δ_T are the biggest contributors to the total electric delay in the secondary path, δ_E. A faster sampling frequency, f_s, will reduce both of these delays. As the sampling frequency is raised, more samples will be needed to the

cover the same response length in the impulse responses used to model the different paths in the controller. This creates a upper limit when choosing the sampling frequency. A rule of thumb says ten times the highest frequency of interest is a good compromise when choosing f_s [3].

2.4 Signal analysis

The influence of the training signal used in the LMS-update process will be presented in this chapter. This chapter was used to analyze the difference in results obtained from the offline and online controller. The transfer paths needed to calculate the offline control filter was measured using white noise and the calculations were performed using a white noise training signal. In the online controller the primary transfer path and control filter was identified and calculated respectively using the provided test conditions. The test conditions are non-stationary with an uneven frequency response.

Investigating the influence of the reference signal characteristics on the optimal filter $\mathbf{h}(n)$ in Figure 2.3 and its descent to the optimal value assume a sample based criterion as an approximation of the variance of the error signal $e(n)$, where $\mathbf{x}(n)$ is the reference signal and $d(n)$ is the desired output:

$$E[e(n)^2] \approx= \frac{1}{N+1}\sum_{n=0}^{N} e(n)^2 = \frac{1}{N+1}\sum_{n=0}^{N}(d(n) - \mathbf{h}^T\mathbf{x}(n))^2 \tag{2.26}$$

The error function $e(n)$ is a quadratic function where the minimum is obtained when the gradient with respect to the control filter h is zero as mentioned above. If the signals in the system are ergodic the solution to the cross and auto spectrum will be unique as seen in equation 2.27[8]. Ergodic signals must be stationary and time invariant. The mean of ergodic signal can be calculated using the time average and the auto-correlation of a ergodic signal is a function of how far apart two samples are spaced.[11]. An example of a ergodic process is gaussian white noise.

$$\frac{lim}{N\to\infty}\frac{1}{N+1}\mathbf{R}_{yy}(N) = \Phi_{yy}, \frac{lim}{N\to\infty}\frac{1}{N+1}\mathbf{R}_{yx}(N) = \Phi_{yx} \tag{2.27}$$

If the ergodic condition for the reference signal is meet and the reference signal auto power spectrum is not zero in the desired frequency interval of control, the control filter will converge towards an optimal value:

$$\frac{lim}{N\to\infty}\mathbf{h}(N) = \Phi_{yy}^{-1}\Phi_{yx} = \mathbf{h}_{opt} \tag{2.28}$$

The reference signal frequency spectrum also influence on the convergence towards an optimal solution. By subtracting the optimal filter $\mathbf{h}(n)$ in equation 2.13 from the filter update equation:

$$\mathbf{h}(n) = \mathbf{h}(n-1) + 2\mu\mathbf{x}(n)e(n) = \tag{2.29}$$
$$\mathbf{h}(n-1) + 2\mu\mathbf{x}(n)(d(n) - \mathbf{h}^T(n-1)\mathbf{x}(n)) = \tag{2.30}$$
$$\mathbf{h}(n-1) + 2\mu\mathbf{x}(n)(d(n) - \mathbf{x}^T(n)\mathbf{h}(n-1)) \tag{2.31}$$

And taking the expected value of equation 2.31:

$$\mathbf{h}(n) = \mathbf{h}(n-1) + 2\mu(\Phi_{xy} - \Phi_{yy}\mathbf{h}(n-1)) = (I - 2\mu\Phi_{yy}\mathbf{h}(n-1)) \tag{2.32}$$

The desired convergence to a zero error function will occur if the absolute value of equation 2.32 is smaller then one. Hence the largest eigenvalue in the reference signal limits the value that the step size parameter μ can take to guarantee convergence towards a optimal value. In the same way does the smallest eigenvalue of the reference signal correspond to the slowest convergence rate and the convergence rate is given by $(1 - 2\mu\lambda_M)$ [8].

3

Methods

3.1 Test Conditions

The project was provided with 6 truck test conditions from Volvo to be used to investigate the possibility for implementing active control. The test conditions are 6 different sound pressure measurements recorded on a operating truck inside the intermediate pipe of the air intake system, see table 3.1. The test conditions are noise related to the regeneration process, engine brake and the compressor. Both the regeneration process and the engine brake use the butterfly valve, see Figure 3.1, which chokes the exhaust from the engine and by doing that increases the pressure in the hot side of the engine. Choking the exhaust is beneficial for the regeneration process to burn diesel particles, it also increases the motor resistance that can be used as a engine brake. The compressor, see Figure 3.1, gets clean air from the air intake after it has gone trough the air filter and thus radiates noise into the exhaust.

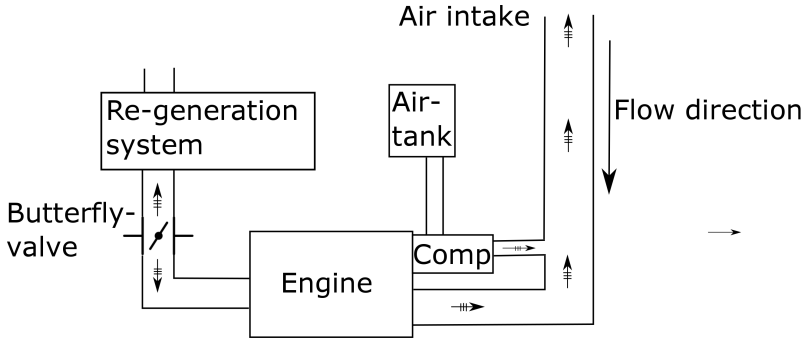

Figure 3.1: Test conditions schematic overview.

Table 3.1: Description of the six test conditions used in the study.

Signal name	**Description**
Butterfly valve on	Engine brake on, Truck coasting down in gear 7
Butterfly valve off	Engine brake off Reference for Butterfly valve on Truck coasting down in gear 7
Normal regeneration	Regeneration with Volvo's current regeneration solution Slow take off, gear 5
New regeneration	Regeneration with Volvo's future regeneration solution Slow take off, gear 5
No Regeneration	No regeneration Reference for regeneration Slow take off, gear 5
Compressor	Compressor on until t=16.5 sec, then compressor off

After analyzing the frequency response of all the recorded test conditions in table 3.1, seen in appendix A a initial control interval was decided to be 20 Hz to 350 Hz. In this frequency range the energy levels are the highest for all the provided test conditions.

3.2 Rig at Chalmers

A prestudy was undertaken on a small test rig at the department of technical Acoustics at Chalmers. This was done in order to get acquainted with how a active noise controller can be implemented on a duct in different frequency ranges.

3.2.1 Setup

The setup at Chalmers is a duct made from a folded 50 mm in diameter PVC pipe with a approximately cut-off frequency for plane wave plane propagation at 944 Hz, see Figure 3.2.

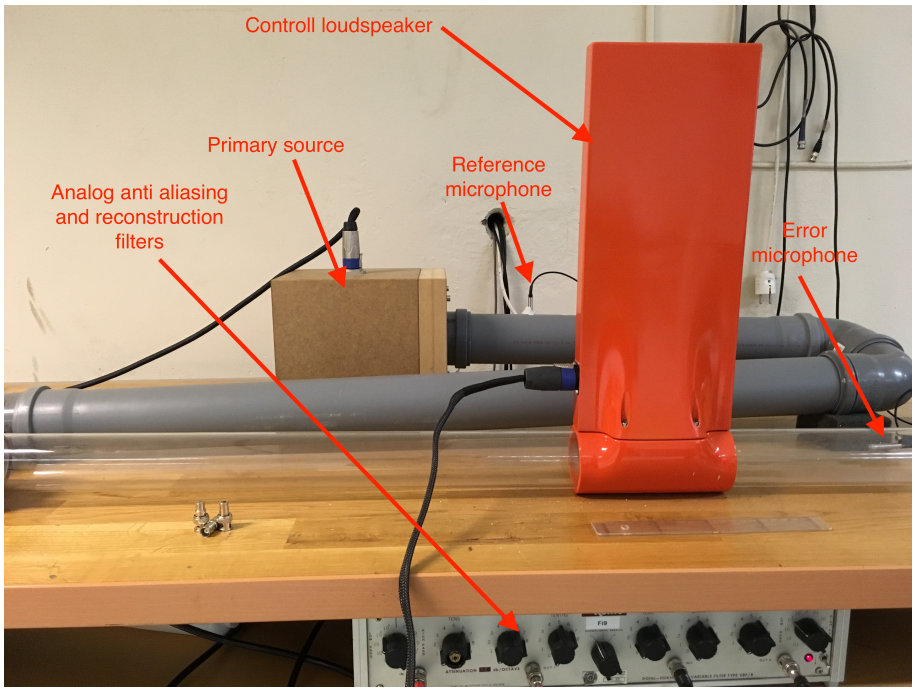

Figure 3.2: Test-rig at Chalmers laboratory.

A speaker is mounted in one end as a primary source and a control loudspeaker is mounted on the pipe 280 cm away from the primary source. The other end of the duct is open. The total length of the duct is 312 cm. The reference and error microphone for the controller were located 13 cm respectively 304 cm cm from the primary source in the duct. The distance between reference microphone and control loudspeaker is 267 cm. The location of the control loudspeaker and the microphones is shown in Figure 3.3.

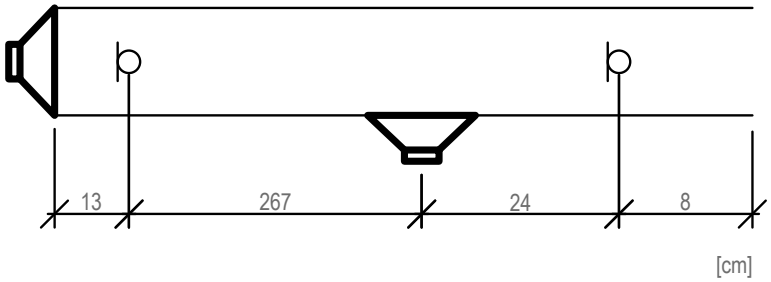

Figure 3.3: Location of control loudspeaker and microphones on the test-rig at Chalmers.

3.2.2 Measurements

Measurements where carried out with and without control with the error microphone at it's original location. Disturbance signals used were stationary white noise signals

and the six test condition signals provided by Volvo. No measurements where done for online control since this controller was still in development at that stage. Prior to playback the test conditions were inverse filtered with the inverse function between the primary loudspeaker and the reference microphone.

This was done in order to remove the influence of the pipe at the Chalmers rig on the test condition signals. The test condition signals were measured in the air intake pipe of the truck and thus are already filtered with the transfer function between the engine and the position they were measured in. By inverse filtering the signals with the transfer function between the primary loudspeaker and the error microphone, the influence of passing trough the duct at the Chalmers rig was removed from the signals.

3.2.3 Simulations in Simulink

The control filter implemented in the duct at Chalmers was a filter calculated using the FxLMS algorithm. The same control filter that was implemented in the duct was also uploaded to a Simulink model. The virtual controller in Simulink was used to investigate the performance of the controller and to verify that there was unity gain over the controller for all frequencies of interest, due to the internal feedback compensation discussed in 2.2.4. The Simulink model is built on the transfer functions information between the two microphones in the duct, between the controller and the error microphone and the feedback path between the controller and the reference microphone in the duct. The simulated reduction and gain over the controller from the Simulink model can be seen in Figures 3.4 and 3.5 respectively in the frequency range 50 Hz to 500 Hz. It can be seen in Figure 3.4 that a good simulated reduction was simulated of at least 15 dB in the whole frequency range was obtained for the offline controller.

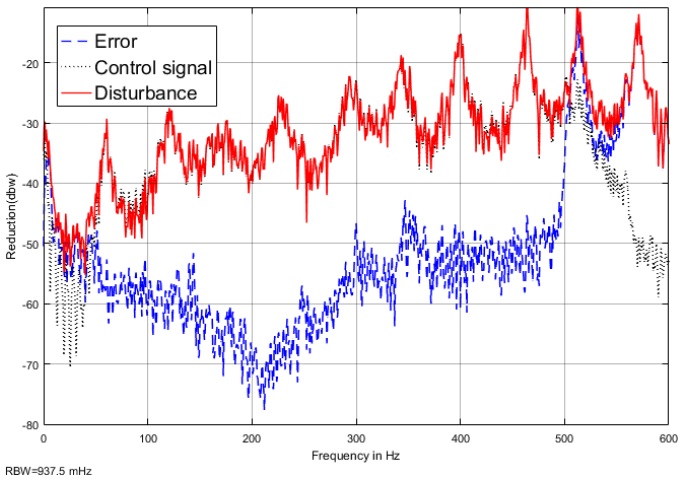

Figure 3.4: Reduction in Simulink model, white noise, 50-500 Hz

In Figure 3.5 it can be seen that there was no offline controller gain except small deviations at 50 Hz and around 400 Hz to 500 Hz.

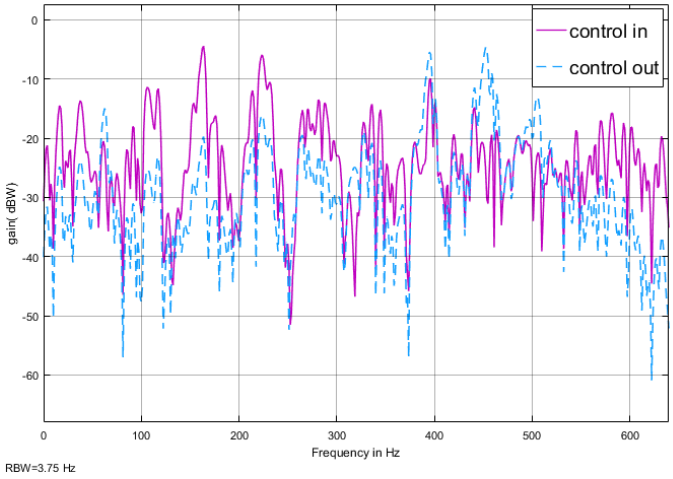

Figure 3.5: Controller gain in Simulink, white noise, 50-500 Hz

3.2.4 dSpace, Control Desk

The digital signal processing unit(DSP) used is from dSpace. The DSP comes with a software, Control Desk, that can be used to monitor the amplitude of the signals in the system in real time uploaded to the DSP. dSpace was used to monitor the controller gain by measuring the in and output signals to the digital controller.

3.3 Rig at Volvo

The complete air intake from a truck was mounted on a aluminum rig to hold the inlet system up for the study, see Figure 3.6. Both offline and online control was implemented on the rig in the modal analysis room at Volvo trucks in Lundby, Göteborg.

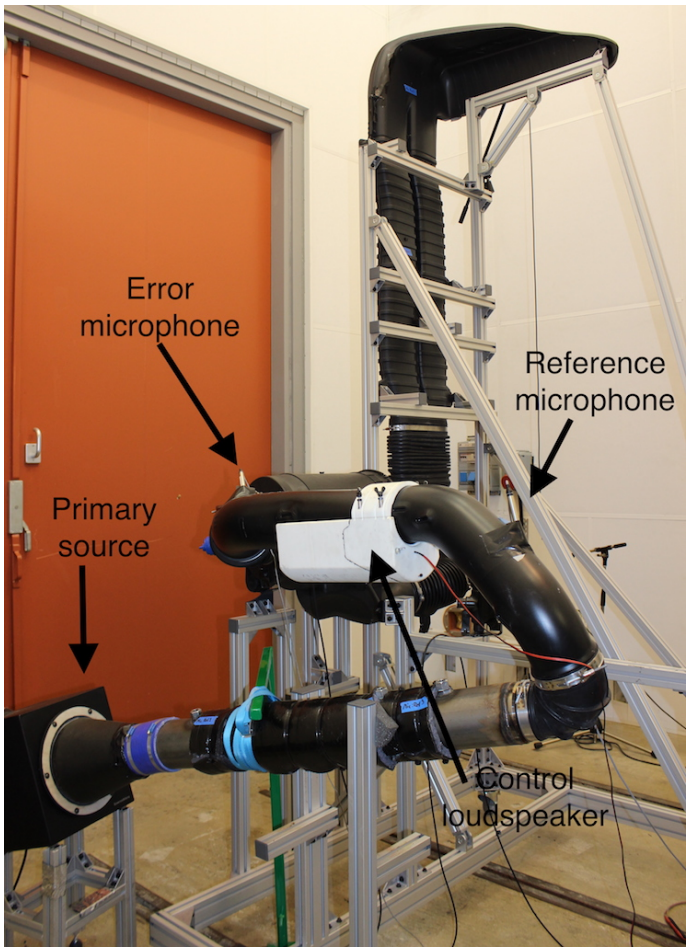

Figure 3.6: The complete air intake mounted on a aluminium rig.

3.3.1 Setup

On an actual truck there is only a small part of the air intake system were there is space to implement a active noise control system. The part of the air intake system were the microphones and control speaker could be mounted was a plastic part called the intermediate pipe, located in the middle of intake system between the air-filter and the turbo inlet seen in Figure 3.6. The short length of the intermediate pipe puts some restraints on the design of the system as mentioned in Section 2.3.

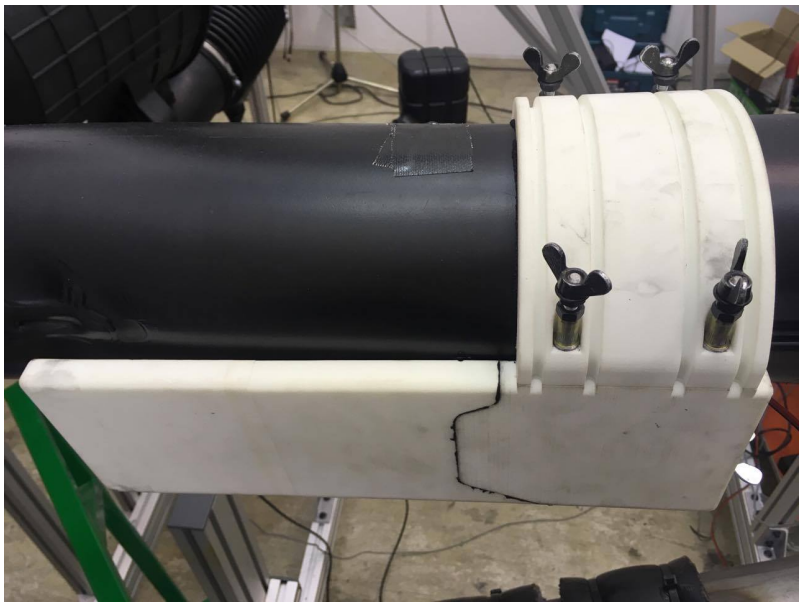

Figure 3.7: Control loudspeaker mount.

The control loudspeaker to be used in the control system was provided by Volvo. The control loudspeaker was a closed boxed design with a volume of four liters. The driver was a four inch piston driver from Visaton, see appendix D for properties. The loudspeaker was designed to fit around the duct and held into place with an extension that goes around the duct with four screws as seen in Figure 3.7.

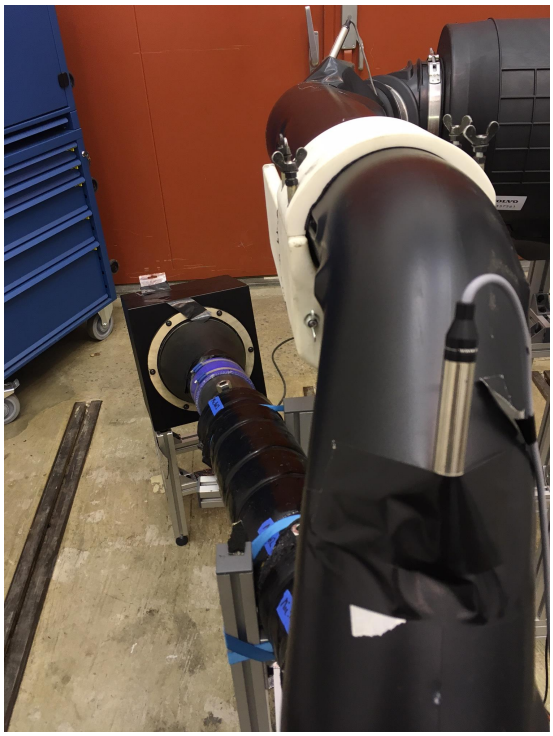

Figure 3.8: Experimental setup and mounting of microphones and primary loudspeaker.

Inspection of the loudspeaker showed that a proper mounting between the driver and the loudspeaker box was missing so a new mounting plate in steel was constructed and installed to firmly hold the driver in position, see Figure 3.9. A half centimeter thick rubber plate was also inserted in between the speaker box and duct to make the coupling between the two as airtight as possible without introducing unwanted losses in the secondary path due to the rubber.

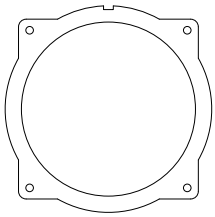

Figure 3.9: Steel plate mounted between speaker driver and box.

The microphones used to implement the controller were two probe pressure microphones type 4182 from Brüel & Kjær, see Figure 3.10. The probe microphones minimize the microphones influence on the acoustic field in the duct and were easy to use and install.

Figure 3.10: Probe microphone used in the project, 4182 from Brüel & Kjær.

The probe of the microphone was inserted into the duct and the microphone housing was held in place using scotch tape with some foam layer inserted between the housing and duct to reduce unwanted vibrations seen in Figure 3.8 . A sub woofer from B&W type CT SW10, see appendix E, was used to generate a acoustic field in the duct and was placed were the engine intake should have been located on the truck. As seen in Figure 3.8 and 3.6 the sub woofer was mounted on a stool half a meter above ground with a horn over the driver to guide the generated wave front into the intake system.

3.3.1.1 Microphone and control loudspeaker locations

In Figure 3.11 frequency response maps of the air inlet system is shown. It can be seen that the air intake system between the engine input and air filter output is resonant and lightly damped. The microphone and control loudspeaker locations were investigated using transmissibility measurements and a frequency response function(FRF) of the air intake system respectively. The finite element frequency response maps of the inlet system seen in Figure 3.11 was provided by Volvo.

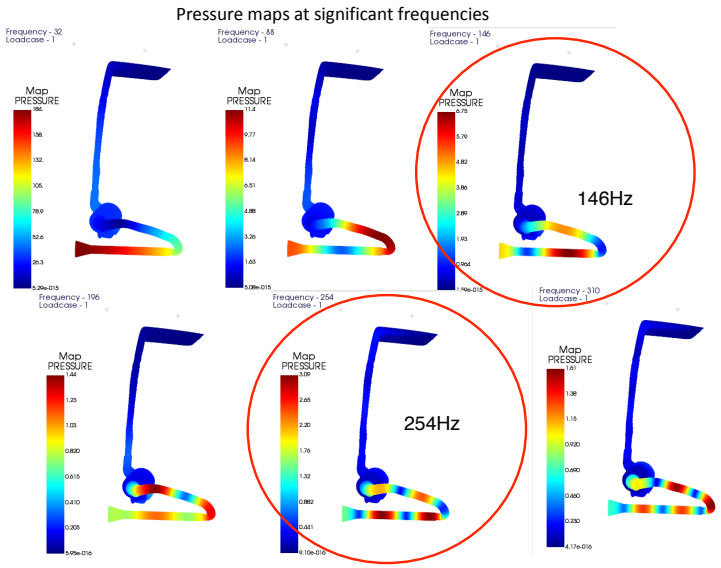

Figure 3.11: Pressure maps

After inspection of the air inlet systems FRF and by looking at spectogram graphs of the test conditions in Figures A.1 to A.6, seen in Appendix A, a new control interval was defined. The new control interval was chosen to be in the frequency range 100 Hz to 350 Hz due to a high energy content around 150Hz and 250Hz seen in the spectrograms graphs for all the test conditions. These frequencies are resonances in the intermediate pipe, seen in Figure 3.11 at 146 Hz and 254 Hz, and appear as strong lines cutting through the spectral lines in all test conditions. The cut-off frequency for plane wave propagation in the intermediate pipe was also investigated and was found to be 380Hz, well above the highest frequency in the new control interval.

The control loudspeaker should be placed in a anti node location on the intermediate pipe that allows the control loudspeaker to maximize the displacement of air inside the duct. Due to lack off spacing there were only two control loudspeaker locations investigated in the duct seen in Figure 3.12.

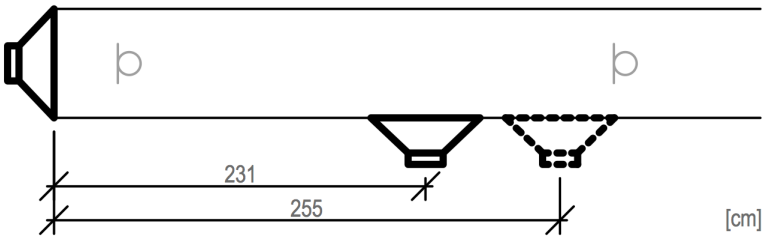

Figure 3.12: Final position of speaker solid line, preliminary speaker position doted line.

In Figure 3.13 it can be seen that if the control loudspeaker was positioned in it's

first position 255 cm from the noise source on the duct the frequencies around 250 Hz would be very hard to control because the control loudspeaker is located at a node at that location in the duct. To move air inside the duct at 150 Hz would not be a problem at this location. If the control loudspeaker was positioned in it's second position 231 cm from the primary source the control loudspeaker would be able to displace the air inside the duct at both 150 Hz and 250 Hz.

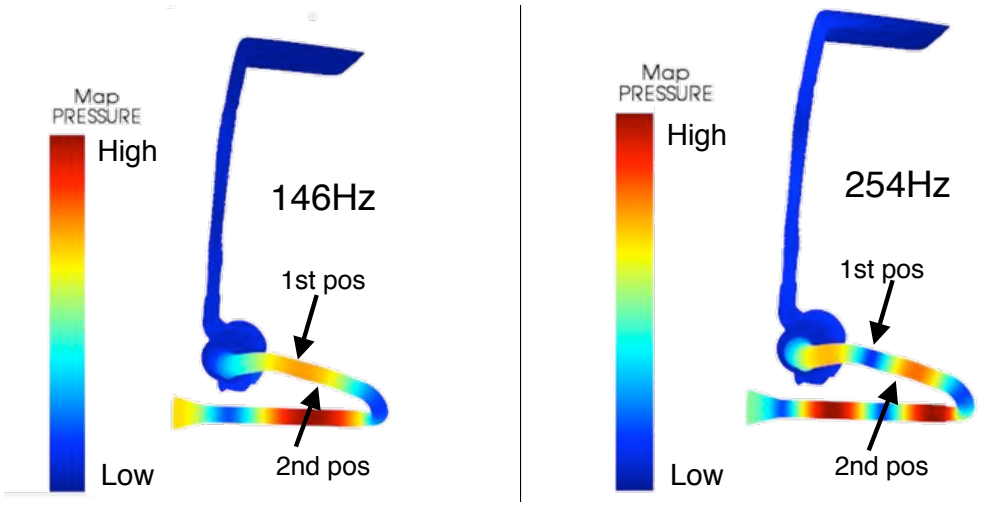

Figure 3.13: Pressure maps for 146Hz and 254Hz for the intermediate pipe with approximate control loudspeaker locations labeled.

To provide the controller with the right frequency response function for control the microphones was also positioned at anti-node positions in the duct, initially the two microphones in the duct were spaced at multiples of 1.13 m and 0.68 m, half the wave length of 150 Hz and 250 Hz respectively from the noise source. Numerous measurements were then performed to find the optimal placement of both the microphones to provide a good FRF for the controller in the frequency interval of interest. In Figure 3.14 the final location of the microphones is shown and in Figure 3.15 the final primary path magnitude and phase response between the two microphones can be seen.

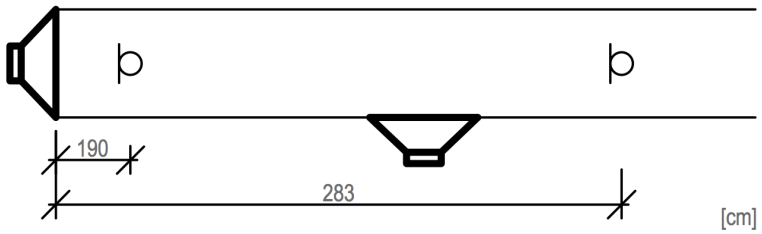

Figure 3.14: Microphone positions.

The primary path magnitude response response is showing a acoustic response of the air intake system at both 150 Hz and 250 Hz with a smooth phase response from 140 Hz to 260 Hz.

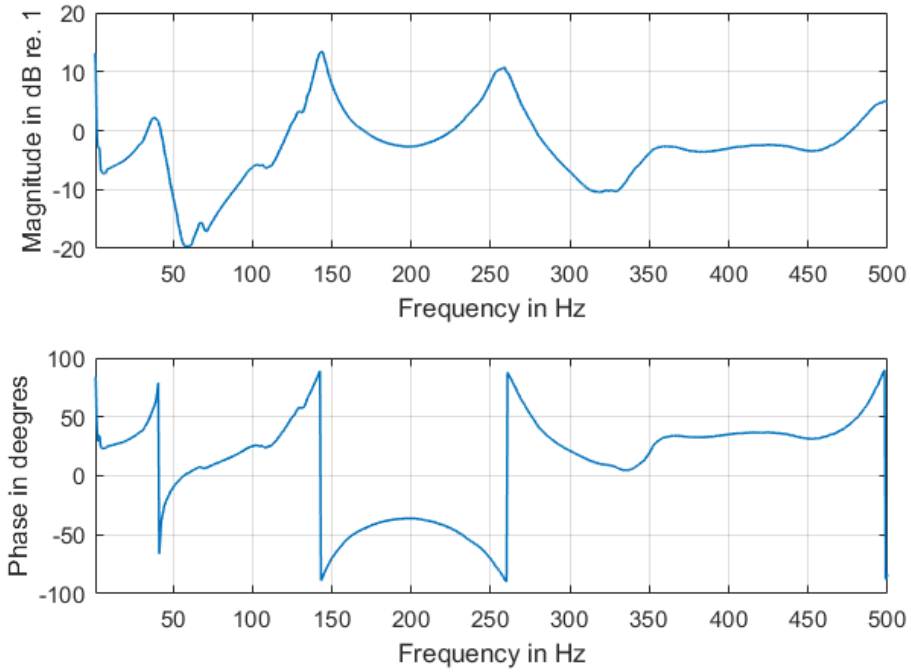

Figure 3.15: Primary path Bode-plot

3.3.1.2 Delay

As described in Section 2.3, the propagation time for the speed of sound from the reference microphone to the control loudspeaker , l_i/c, needs to be larger than the electrical delay δ_E, where l_i is the distance between reference microphone and the speaker. In practice this condition can be translated as: the delay in primary path has to be equal or larger than the delay in secondary path.

Because the part of the air intake were ANC could be implemented was of limited length the delay in the the secondary path was initially larger then the delay in the primary path which is 14 samples or 2.7 ms. The delay in the secondary path was measured and it was determined that the easiest option would be to change the analog anti aliasing and reconstruction filters to less steep filters with less delay. Initially a 48 dB/octave analog filter was used with a cut-off frequency set to 2 kHz which according to equation 2.24 in Chapter 2.3 has 3 ms or 15.36 samples of delay. With the 48 dB/octave filter the total delay in the secondary path was measured to 22 samples. By changing the analog filters to 24 dB/octave with the same cut-off frequency, the delay in the analog filters was reduced to eight samples and the total delay in the secondary path was measured to 15 samples. Finally to get below the delay in primary path the filters were changed to 12 dB/octave which only had 1.25 kHz as an option for the cut-off frequency. These filters have a delay of 6 samples or 1.2 ms and the total delay in secondary path was now measured to be 13 samples which is 1 sample or 0.19 ms less then in the primary path which was considered sufficient.

By looking at the measured impulse responses for primary path and secondary path in the final setup, the difference in delays could be estimated to one sample long, indicating a causal system, see Figure 3.16 and 3.17 .

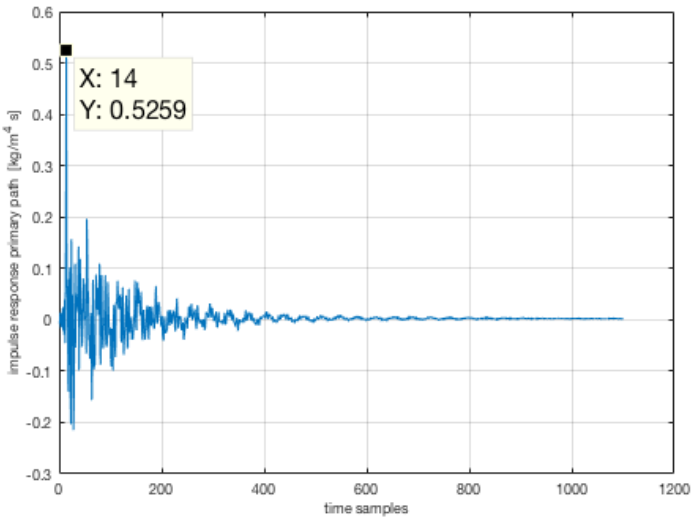

Figure 3.16: Delay in impulse response primary path.

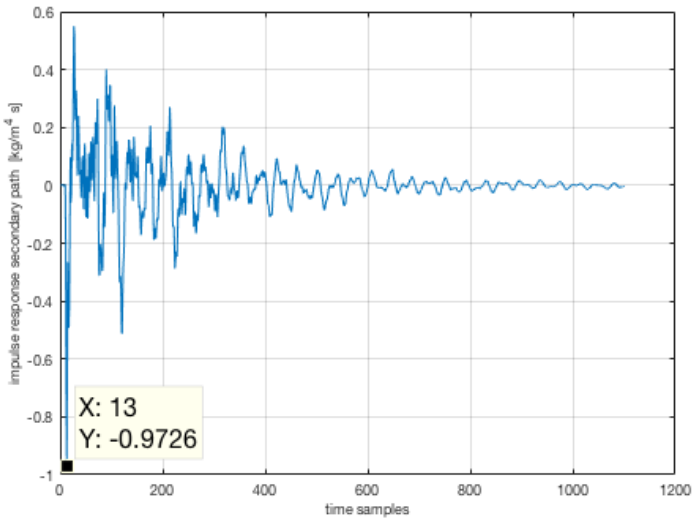

Figure 3.17: Delay in impulse response secondary path.

3.3.2 Measurements

Measurements measuring the reduction the ANC system has on the signals that is with and without control were carried out with both stationary white noise and the 6 test conditions provided for the Volvo truck. The test conditions were inverse filtered to remove the influence of the laboratory air intake system on the recorded test conditions, knowing that the test conditions were measured close to the location of the reference microphone on the duct. The FRF between the input of the primary source and the reference microphone was used to inverse filter all the test conditions. All white noise reduction measurements were carried out with and without control using the error microphone, seen in Figure 3.14. Three sensors were used in the final test condition reduction measurements with and without control; a accelerometer located on the aluminum rig(passive side), a accelerometer located on the inlet pipe(active side) and finally one microphone positioned at the inlet pipe mouth seen in Figures 3.18a and 3.18b respectively. Reduction measured with the error microphone was recorded using the VXI acquisition station together with the software program Trigger Happy. The test condition measurements were recorded with Squadriga recording system and Artemis software from Head Acoustics.

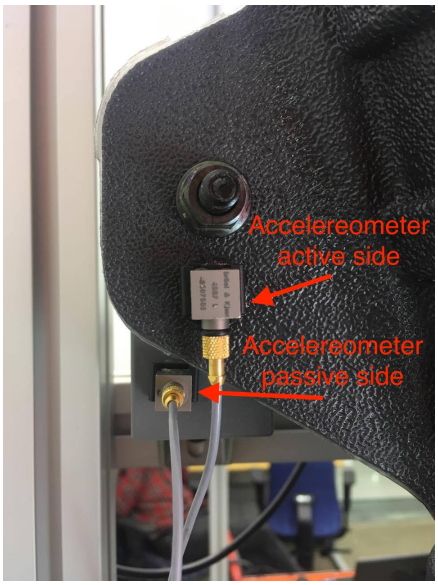

(a) Accelerometer placement on test-rig

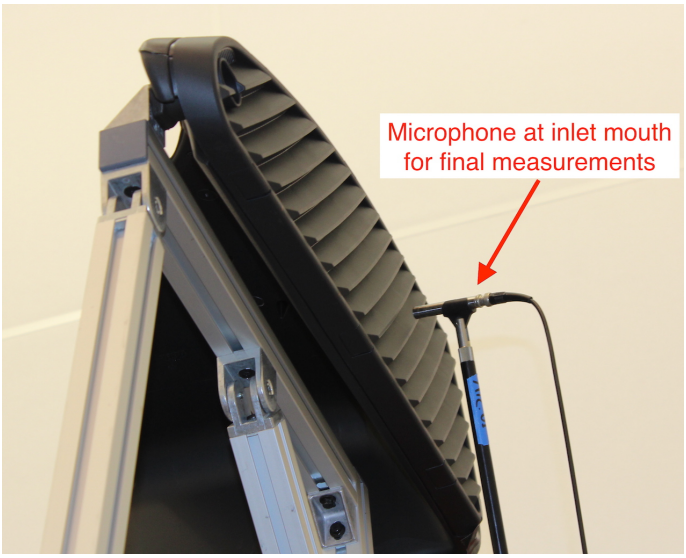

(b) Inlet measurement microphone placement on test-rig

Figure 3.18: Sensor locations on test-rig for the test conditions measurements

A measurement was carried out to calculate the displacement and power consumption of the control speaker during control of the six different test conditions. The acceleration measurements were carried out with a accelerometer glued to the diaphragm of the control loud speaker, see Figure 3.19a. The voice coil displacement was calculated by integrating the voice coil acceleration data. Power consumption of the control loudspeaker was calculated by measuring the voltage drop over a small shunt resistance place in series with the loudspeaker to obtain the current drawn by the loudspeaker and by measuring the voltage over the loudspeaker terminals. The measurement setup is shown in Figure 3.19b. The current drawn by the loudspeaker is then $I = V_2/R$ and the power is $P = IV_1$. Acceleration, voltage and pressure measurements were recorded using the VXI data acquisition station.

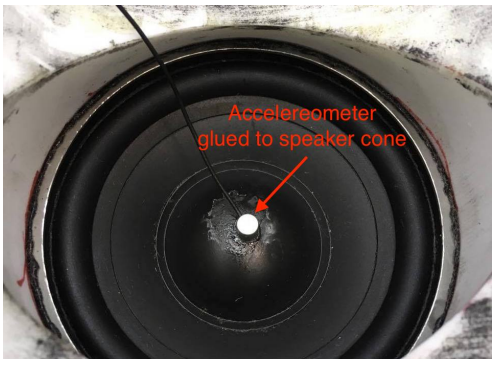

(a) Mounting of accelerometer on speaker cone

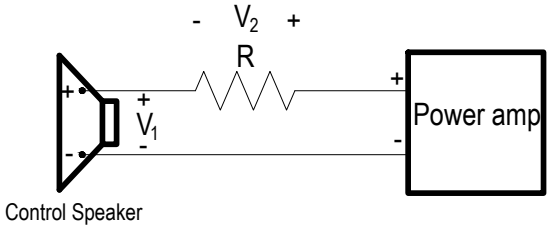

(b) Schematic of speaker power measurement.

Figure 3.19: Setup for measuring power consumption of speaker and acceleration of the diaphragm.

3.3.3 Simulation in Simulink

A Simulink model was built in order to simulate reduction and gain of the controller system. The models served as a development tool and was convenient for debugging and testing of the system. As in the offline Simulink model at Chalmers the measured transfer functions for primary, secondary and feedback transfer path were imported into the virtual model to serve as representation of the physical transfer paths.

3.3.4 Offline implementation

The first controller to be implemented was an offline FxLMS controller. The controller was implemented using three transfer functions $P(j\omega)$,$C(j\omega)$ and $F(j\omega)$. The first one is located between the reference microphone and the error microphone(primary path), the second one is between the input of the controller and the error microphone(secondary path) and a feedback transfer function between the control loudspeaker and the reference microphone. The transfer functions were measured with white noise as reference signal. The obtained transfer functions were then transformed to impulse responses to calculate the control filter as described in section 2.2.3.1. The obtained control filter and the impulse response for the feedback path are then uploaded to the DSP. The offline setup is shown in Figure 3.20

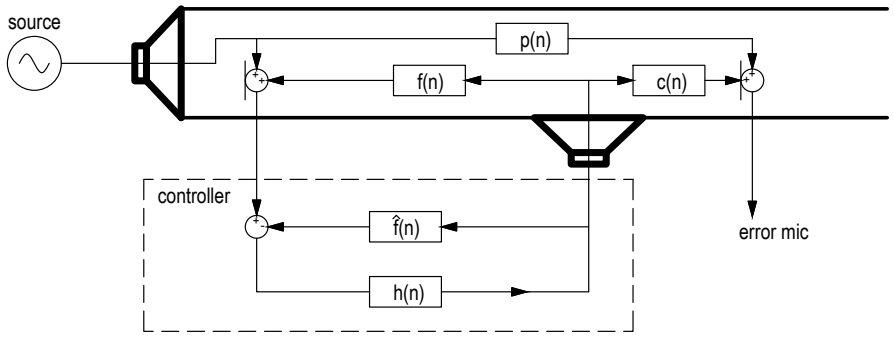

Figure 3.20: Setup for the offline controller.

3.3.5 Gain

There were two gain obstacles encountered in the implementation process of the controller. One gain issue was identified to arise from the the feedback neutralization method used discussed in 2.2.4. The problem was solved by moving gain from the controller to the control loudspeaker amplifier. The second obstacle was that the control loudspeaker was not able generate high enough sound pressure levels to cancel the true sound pressure levels of the measured test conditions in the intermediate pipe. Further analysis on the achievable control speaker levels can be read

in section 3.4 below.

3.3.6 System identification

System identification of the transfer functions for secondary path and feedback path are estimated using the LMS algorithms. White noise that is uncorrelated with the primary source noise is injected from the DSP trough the control loudspeaker to act as reference for the estimation, see Figure 3.21.

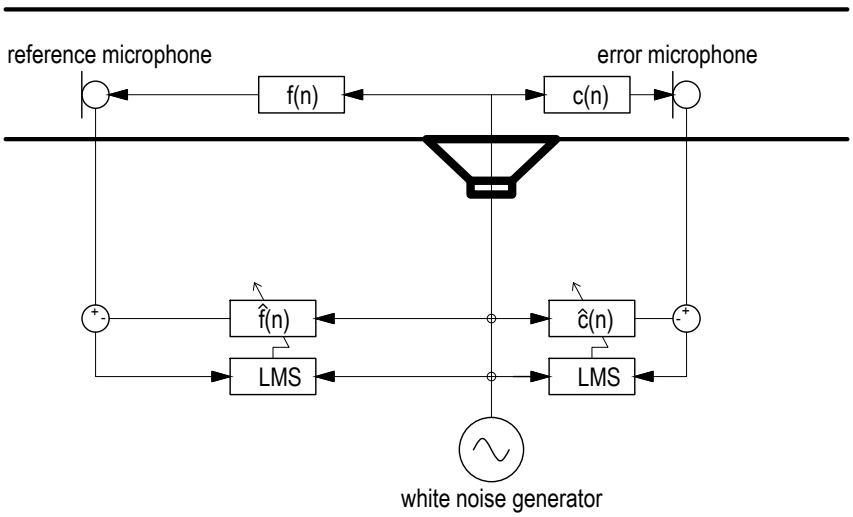

Figure 3.21: Setup for open loop estimation of secondary and feedback path.

Both open loop and closed loop system identification configurations were developed. In the open loop configuration the impulse responses $\hat{\mathbf{c}}(n)$ and $\hat{\mathbf{f}}(n)$ are estimated prior to control and primary noise being turned on. In the closed loop configuration the necessary impulse responses, $\hat{\mathbf{p}}(n)$, $\hat{\mathbf{c}}(n)$ and $\hat{\mathbf{f}}(n)$ are estimated when the primary source is radiating sound into the duct. In this arrangement it is possible to track changes in the transfer functions over time while the system is operating. The secondary transfer path is modelled in closed loop arrangement by subtracting the contribution of the primary path noise from the secondary path update equation [3].

3.3.7 Closed vs open system identification

In this section system identification for both closed and open loop arrangement of the secondary and feedback path will be presented. Estimation signals is filtered in the controller by a low-pass Chebychev type one minimum phase filters with a cut

off frequency of 350 Hz. The estimation results will be shown together with estimations on the actual air intake system by the controller against estimations obtained in Simulink simulations and from measurements of the transfer paths, obtained using the VXI-workstation. Comparison of the open-loop system identification and measurements for the secondary and feedback path, can be seen in Figures 3.22 and 3.23.

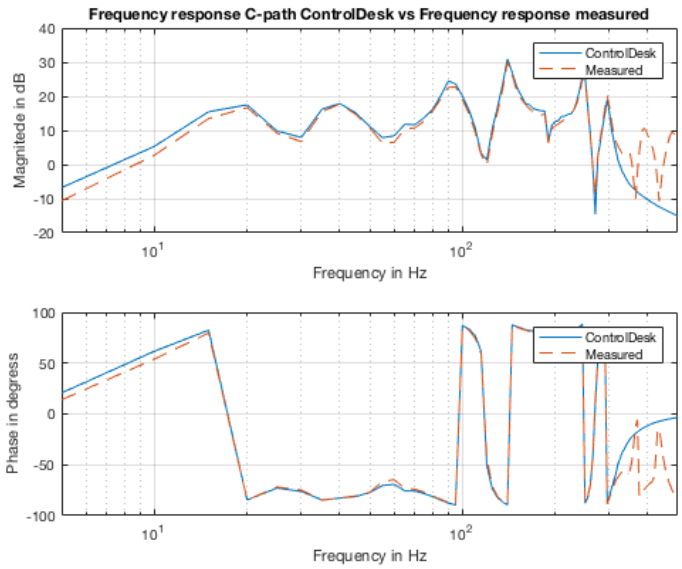

Figure 3.22: Open-loop secondary path estimation vs measured secondary path

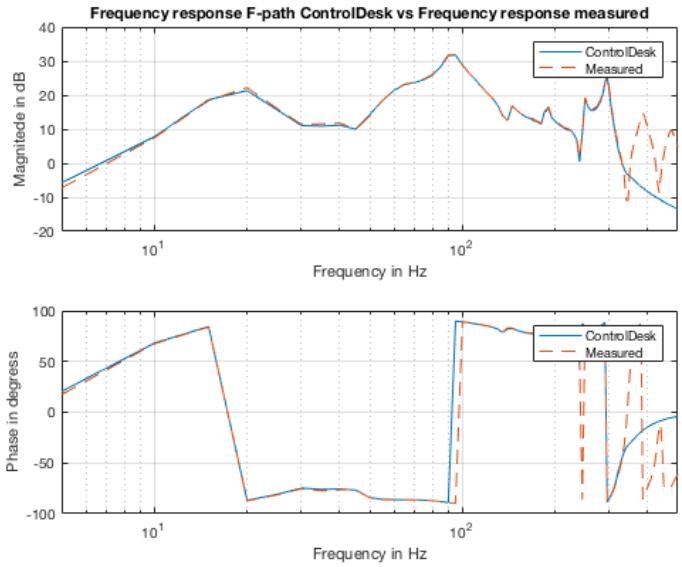

Figure 3.23: Open-loop feedback path estimation vs measured secondary path

In an open-loop arrangement it can be seen that both the estimated secondary and feedback path are well estimated by the controller in the control interval 100 Hz to

350 Hz. A small deviation in the estimated and measured phase response can be seen at 250 Hz for the feedback path in Figure 3.23.

Comparison of the closed-loop estimation of the secondary and feedback path by the controller against measurements can be seen in Figure 3.24 and 3.25 respectively.

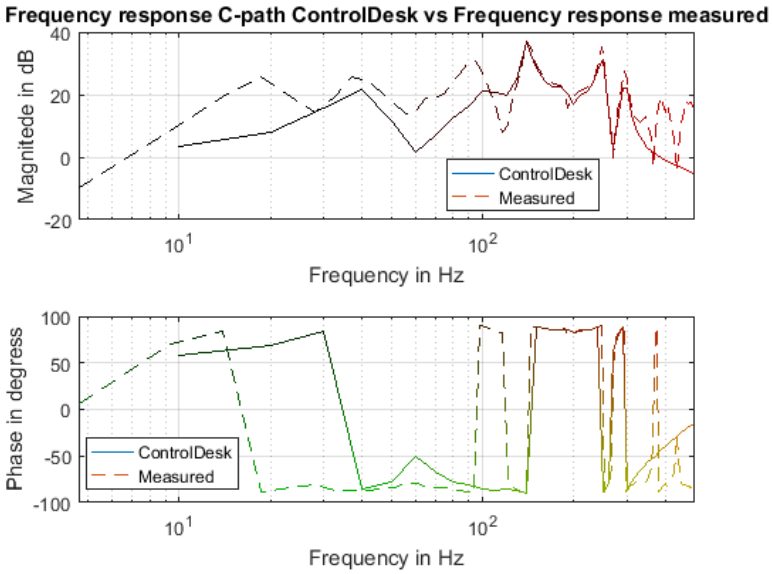

Figure 3.24: Closed-loop secondary path estimation vs measured secondary path

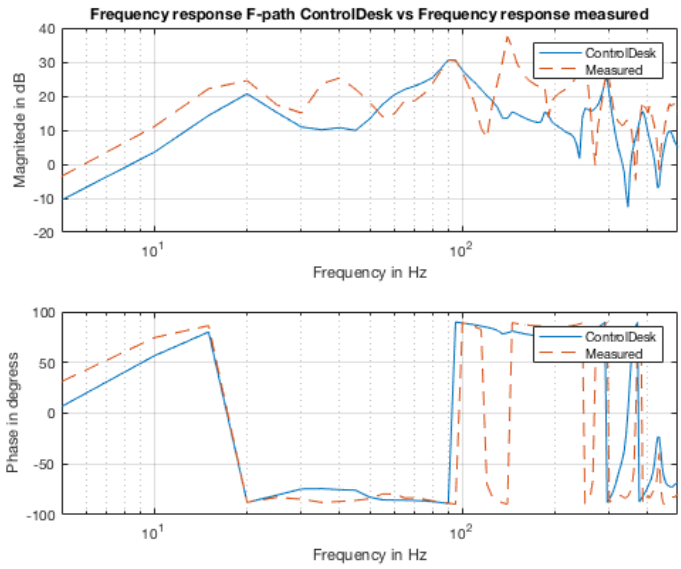

Figure 3.25: Closed-loop feedback path estimation vs measured feedback path

In Figure 3.25 it can be seen that the feedback path could not be estimated in a closed-loop configuration in the control interval 100 Hz to 350 Hz. The secondary

path estimation looks fine from about 150 Hz to 350 Hz. The reason for the poor estimation of the feedback path could not be identified but a gain issue is suspected. Simulated estimations performed in Simulink of the same controller as the one uploaded to the DSP obtained a good estimation of the feedback path for the closed-loop setup in the whole control interval, seen in Figure 3.26 below.

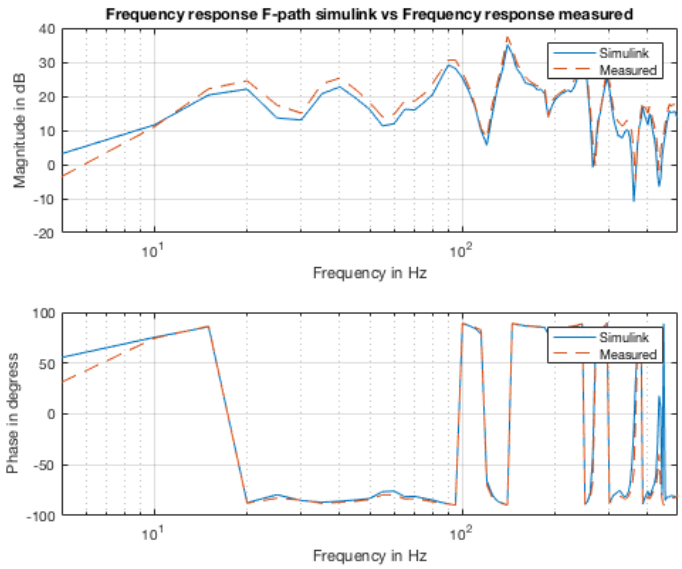

Figure 3.26: Simulink vs measured feedback path

From the results shown in this section it was decided that closed loop system identification was not going to be implemented due to stability issues arising from poor estimation of the feedback path. In the rest of the report when referring to a online controller this will refer to a online controller in a open-loop configuration.

3.3.8 Online implementation

After the offline controller was successfully implemented, a online controller was constructed, see Figure 3.27.

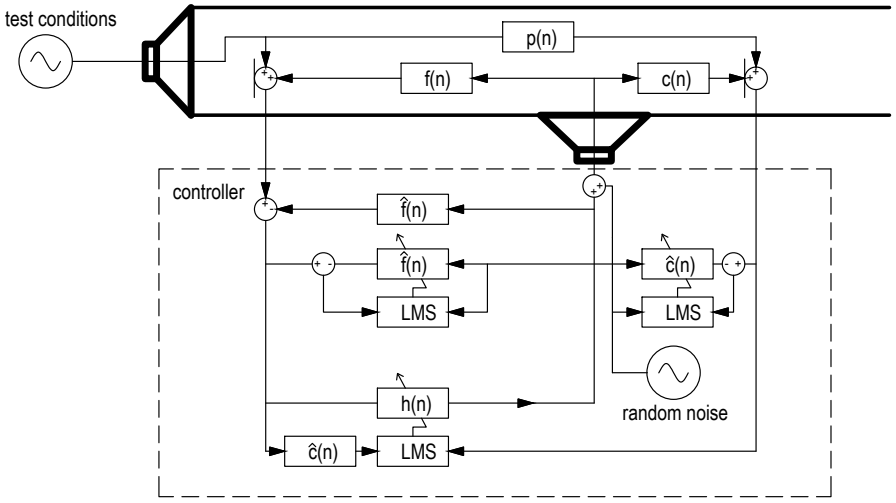

Figure 3.27: Online setup.

The necessary transfer function identification for the online controller was implemented using the LMS system identification algorithm, logic networks, appropriate error sensors and the control loudspeaker. To improve the speed and performance of the online controller the digital linear phase band-pass filters used in the offline controller to filter the reference signal were switched to band-pass Chebychev type one minimum phase filters.

Different kinds of filter lengths for the identification of the secondary transfer path, feedback transfer path and controller were also investigated. Reasonable identification of the feedback and secondary transfer functions, was obtained with 1024 filter coefficients. For the controller a shorter filter gave the best result, 256 filter coefficients. Initial conditions were used to reduce convergence time, both for the identification and the control filter. This reduced convergence time significantly. The initial conditions were carried out such that the filter coefficient values from last run were stored as initial conditions for next run.

3.4 Speaker analysis

The control loudspeaker seen in Figure 3.7 is of a undamped closed box loudspeaker design with a frequency response function of a single degree of freedom system(single-DOF). The control loudspeaker is fitted with a loudspeaker woofer of compact size and a low resonance frequency from Visaton, see appendix D. The combined combined loudspeaker box and woofer's resonance frequency was measured to be 70 Hz, see Figure 3.28. The electrical impedance of the control loudspeaker was measured with a Clio measurement system with the control loudspeaker standing on the floor on top of some damping material in the laboratory room.

The volume of air that needs to be displaced by the control loudspeaker depends on the required sound power and frequency. The amount of air displaced by a piston loudspeaker is a product of the loudspeakers diaphragm excursion and diaphragm area. In general the larger the loudspeaker diaphragm is the greater volume of air is moved by the loudspeaker. The displacement as a function of frequency for a loudspeaker with a single-DOF can be divided into three frequency regions, below the loudspeaker resonance frequency, at loudspeaker resonance frequency and above the loudspeaker resonance frequency. Below the loudspeakers resonance frequency the displacement of the loudspeaker diaphragm is fairly constant, at the loudspeaker resonance frequency the displacement is controlled by the loudspeakers electrical and mechanical damping and above the resonance frequency the displacement of the loudspeaker diaphragm is that of a second-order low-pass filter slope [12].

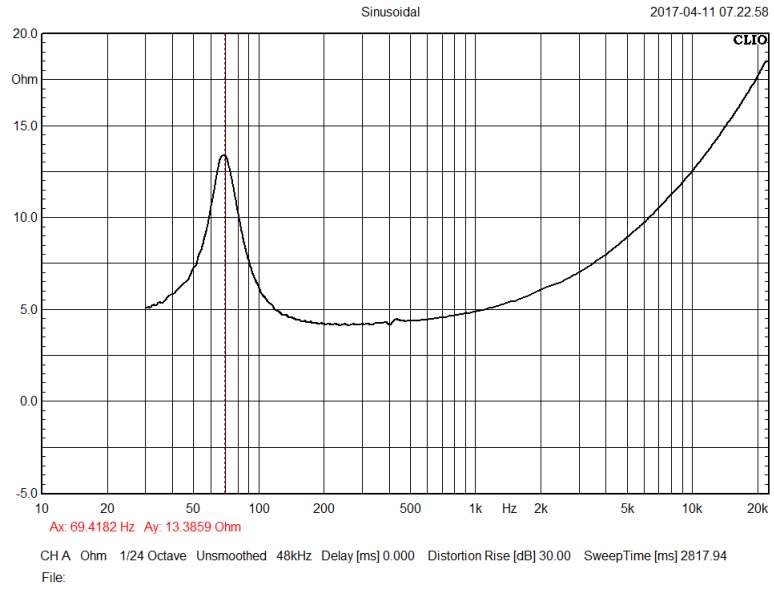

Figure 3.28: Electrical impedance, control loudspeaker

A loudspeaker electrical power consumption is related to the voltage magnitude over the loudspeaker input and the voice coils winding resistance in ohms. To lower the electrical power consumption of a loudspeaker the voice coil wire resistance and the number of voice coil wire turns should be low.

One way to reduce both the loudspeaker diaphragm excursion and the electric power consumption for a given sound pressure level at low frequencies is to use a loudspeaker with a big diaphragm area. This allows for a greater volume of air to be moved for a given loudspeaker force factor. When a big diaphragm loudspeaker is not an option due to size and a loudspeaker with a small diaphragm area is used to generate low frequencies a overhung voice coil geometry is usually used. Comparing the control loudspeakers voice coil height (7 mm) and front pole plate height(3 mm), seen in appendix D it seems that the control loudspeaker provided by Volvo for the project is a overhung design loudspeaker. Overhung voice coil geometries usually

allow for large loudspeaker voice coil displacements x_{max} [13] to be able to generate greater volume velocities [14]. The trade off using the overhung voice coil geometry is that once the diaphragm passes maximum displacement x_{max} the diaphragm exceeds the loudspeakers uniform magnetic field, the loudspeaker then has little control over the diaphragms movement.

The test conditions provided by Volvo have high sound pressure levels at low frequencies. Knowing that a loudspeaker limitation to produce the required sound pressure levels is due to the displacement of the diaphragm and electric power consumption of the loudspeaker driver respectively. It was therefore doubtful in an early stage if the provided four inch driver would be able to produce the low frequency diaphragm displacement in the initial control interval 20 Hz to 350 Hz. The linear excursion limit x_{max} of the four inch Visaton driver is 8 mm with a electric nominal power of 25 W and peak power of 40 W. It was therefore decided to investigate if there existed a working range where the control loudspeaker could generate the measured sound pressure levels of the test conditions by analyzing the loudspeakers diaphragm displacement and power consumption in the frequency range of interest.

The idea for analyzing the control loudspeaker limitations is to measure the sound pressure at the reference microphone with and without control for couple of different amplitudes in the duct at the same time as the diaphragm displacement and power consumption of the loudspeaker were measured under control. Control was performed for low sound pressure levels where the control loudspeaker was assumed be working within its working range in the initial control interval 20 Hz to 350 Hz. The initial control interval was chosen over the newer control interval, 100 Hz to 350 Hz, to extract more information about the loudspeakers dynamic behavior under control.The obtained diaphragm displacement and power consumption data could then be used together with the measured sound pressure level to extrapolate the results, assuming a linear relationship, up to the the actual test condition sound pressure levels to see if there existed a working range where the control loudspeaker could be used to control the actual test condition sound pressure levels.

In Figures 3.30 to 3.36 the speaker analysis results can be seen for all the Volvo truck test conditions. The graphs are displayed with a cut-off frequency on the horizontal axis and the loudspeaker consumed Power and displacement on the vertical axis. The speaker analyses is displayed as a superposition of the measured displacement and power by summing up the data in intervals of df, df being the frequency resolution of a sampling frequency of 5120 Hz. The cut-off frequency is lowered in each summation step df going from high to low frequencies until the lowest frequency of control is reached using a high pass filter with the summed value of df as a cut off frequency. To analyze the displacement and power consumption of the loudspeaker under control the mechanical aspects of the loudspeaker and the controller frequency response magnitude of the duct needs to be investigated together with the acoustic behavior of the duct itself. In Figure 3.29 the controllers acoustic frequency response function of the duct is shown again for convenience for the reader.

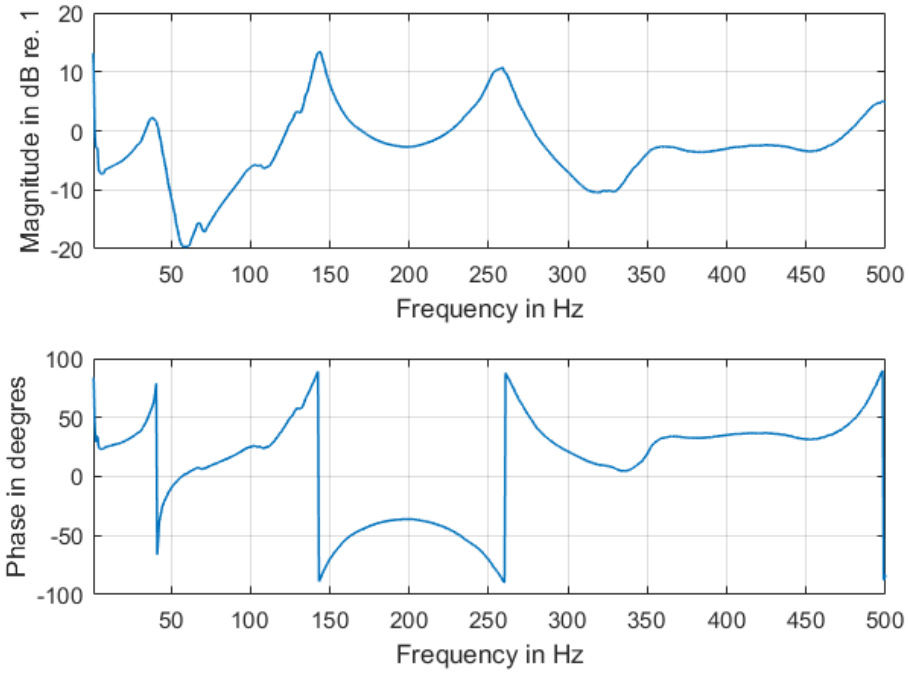

Figure 3.29: Primary path Bode-plot

In Figure 3.30 the speaker analysis is shown for the "Butterfly valve on" test condition is shown. It can be seen that the control loudspeaker would not be able to generate the necessary sound pressure level without violating the power handling capability of the woofer driver for all frequencies of interest. The measured and extrapolated electrical power consumption of the loudspeaker follows the test conditions frequency magnitude fairly well, seen in Figure A.2. The consumed power of the control loudspeaker for the butterfly valve of test condition, seen in Figure 3.30a, indicates that moving the loudspeaker diaphragm at lower frequencies is harder then moving the diaphragm at higher frequencies. Increasing the displacement of the loudspeaker diaphragm should also increase losses.

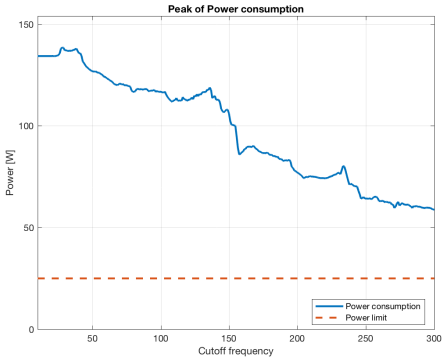

(a) Consumed power over frequency.

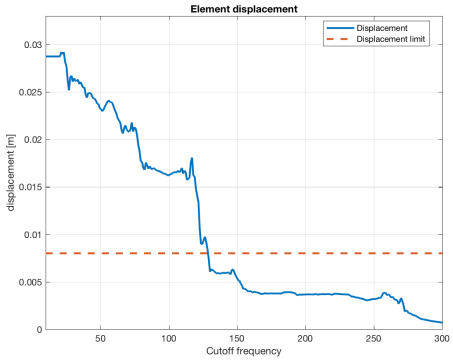

(b) Element displacement over frequency.

Figure 3.30: Results from study on consumed power and diaphragm displacement, Butterfly valve on condition.

The diaphragm displacement of the control loudspeaker for the "Butterfly valve on" test condition is seen in Figure 3.30b. It can be seen that the control loudspeaker can generate the sound pressure level of the test condition for frequencies above 130 Hz without violating the control loudspeakers maximum diaphragm excursion limit. Above 130 Hz the displacement is fairly constant with a low amplitude, following the test condition frequency response magnitude fairly well. Below 130 Hz the diaphragm displacement jumps in magnitude past the maximum diaphragm displacement limit and settles again around the control loudspeakers resonance frequency, this is the frequency range were the frequency magnitude of the "Butterfly valve on" test condition is largest. At 70 Hz the displacement is still increasing, in this frequency range the "Butterfly valve on" test condition magnitude is large but the controller acoustic frequency response function of the duct is low, seen in Figure 3.29. Displacement for a undamped system as mentioned above is only limited by the mechanical and electrical damping of the system at resonance. If the damping at resonance is low the magnitude at resonance due to a small excitation can become surprisingly large. Below the loudspeaker resonance frequency the displacement in figure 3.30b increases with a constant slope as the frequency is lowered. In this frequency region the loudspeaker diaphragm displacement is almost constant. This is the stiffness controlled range in witch the loudspeaker diaphragm displacement is a product of the loudspeaker driving force and the combined compliance of the driver and loudspeaker box [12].

The result for the "Butterfly valve off" test condition is shown in Figure 3.31. The "Butterfly valve off" test conditions violates the control loudspeakers power handling capability in the whole frequency range of interest. The consumed power increases as the frequency goes down as expected. The excursion limit for the loudspeaker diaphragm is violated for frequencies below approximately 40 Hz.

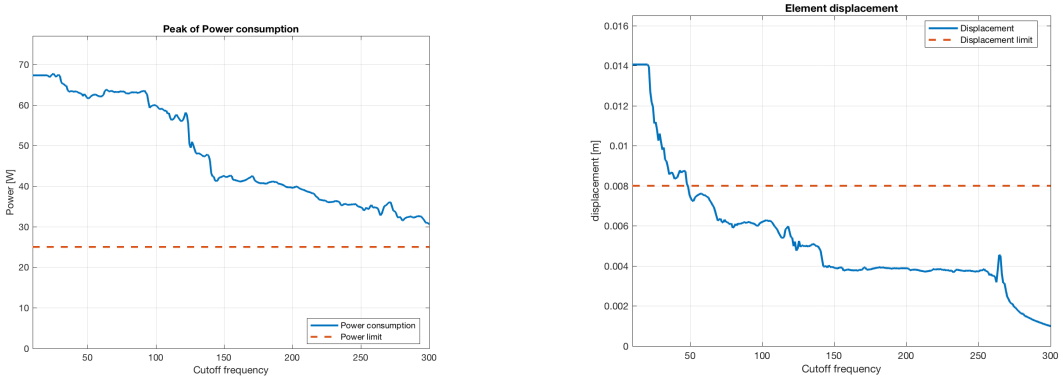

(a) Consumed power over frequency.

(b) Element displacement over frequency.

Figure 3.31: Results from study on consumed power and diaphragm displacement, Butterfly valve off test condition.

The same trend in diaphragm displacement can be seen in Figure 3.31 as in Figure 3.30 for the "Butterfly valve on" test condition. The displacement increases mostly around 130 Hz where the test condition magnitude is largest seen in Figure A.1. Around the loudspeaker resonance frequency at 70Hz the displacement slope increases and then at around 40 Hz the displacement grows rapidly. At 40Hz both the controllers frequency response function and the test condition magnitude is large. This together with the that the controller is working in a nodal point around this frequency in the tube, seen in Figure 3.32 is believed to cause the large loudspeaker displacement seen in Figure 3.31b.

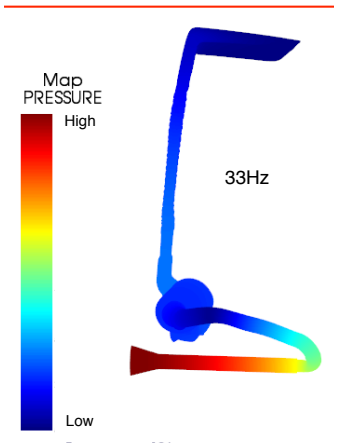

Figure 3.32: Pressure maps for 33Hz in the intermediate pipe.

In Figure 3.33 the loudspeakers consumed power and diaphragm displacement is shown for the "Compressor" test condition. The nominal power consumption of the loudspeaker is violated for a cutoff frequency below 150 Hz and the diaphragm displacement is larger then the excursion limit for cutoff frequencies below 20 Hz. In

the "Compressor" test condition frequency response magnitude, seen in Figure A.3 it can be seen that the test condition have a large magnitude in the range 20 Hz to 40 Hz.

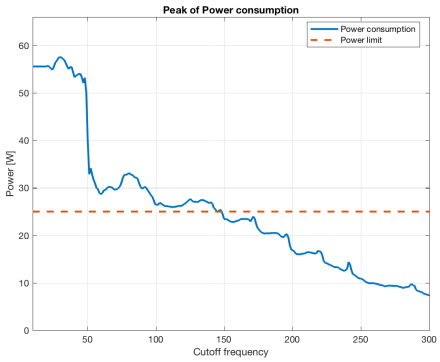

(a) Consumed power over frequency.

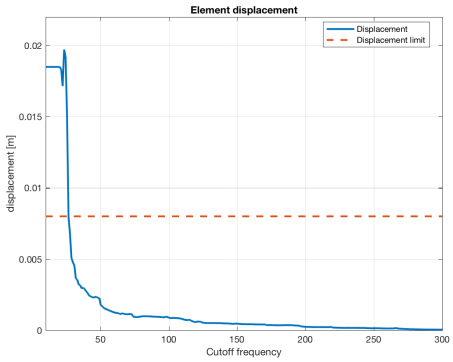

(b) Element displacement over frequency.

Figure 3.33: Results from study on consumed power and diaphragm displacement, Compressor test condition.

By comparing the frequency magnitude of the "Butterfly valve off" test condition in Figure A.1 and "Compressor" test condition in Figure A.3. It can be seen that the "Compressor" test condition is more narrow band then the "Butterfly valve off" test condition. The frequency response magnitude of the "Compressor" test condition is higher then for the "Butterfly valve off" test condition. Yet the consumed power of the loudspeaker for the "Compressor" test condition is lower then for the "Butterfly valve off" test condition. This result seems to indicate that generating narrow band disturbance is easier then generating broadband disturbances for a loudspeaker.

In Figure 3.34 the result for the "No regeneration" test condition is shown. The consumed power is violated in all frequencies of interest for the "No regeneration" test condition. The consumed power follows the test conditions frequency response magnitude seen in Figure A.5.

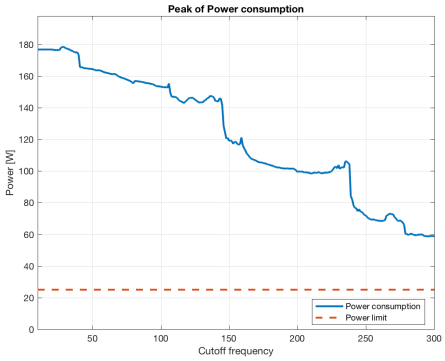

(a) Consumed power over frequency.

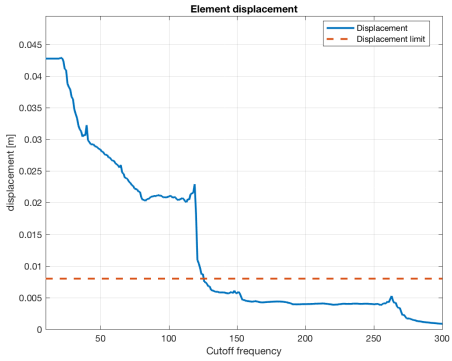

(b) Element displacement over frequency.

Figure 3.34: Results from study on consumed power and diaphragm displacement, No regeneration test condition.

Displacement of the diaphragm for frequencies above 130 Hz does not violate the driver excursion limit. At 125 Hz in Figure A.5 it can be seen in the spectrogram plot that there is a lot of energy in this frequency band. At the loudspeaker resonance frequency it can be seen a shift in the diaphragm displacement slop then a 40Hz the slope displacement increases again. Looking at the test condition frequency response magnitude in Figure A.5 it can be seen that the test condition contain a lot of energy at both 70 Hz and 40 Hz.

In Figure 3.35 the speaker analysis is shown for the "Normal regeneration" test condition. This test condition was one of the test conditions with the highest amplitude. Again the maximum power handling capability of the loudspeaker is violated when the power consumption is extrapolated up to the true test condition sound pressure level. The consumed power of the loudspeaker follows the test condition frequency magnitude seen in Figure A.6. At the loudspeaker resonance the test condition magnitude is the highest, seen in Figure A.6, and the displacement slope is again seen to be raised at this frequency. At 40Hz the same phenomena as before is observed. Causing large diaphragm displacements.

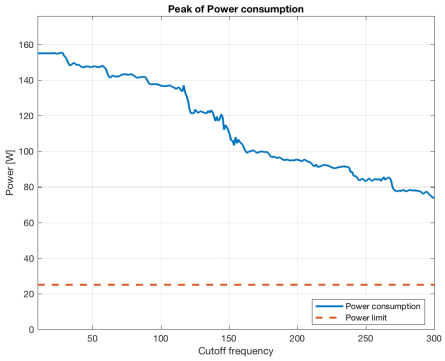

(a) Consumed power over frequency.

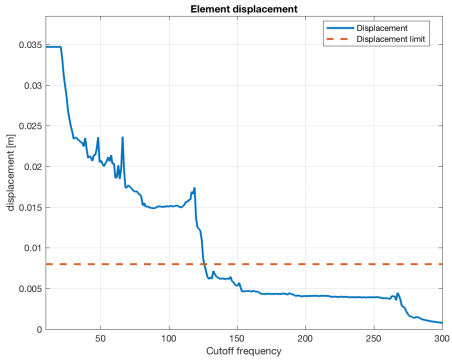

(b) Element displacement over frequency.

Figure 3.35: Results from study on consumed power and diaphragm displacement, Normal regeneration test condition.

In Figure 3.36 the result is shown for the "New regeneration" test condition. This was the test condition with the highest sound pressure level. The consumed power of the loudspeaker follows the frequency response magnitude of the test condition seen in Figure A.4. The consumed power of the loudspeaker violates the power handling capability in all frequencies of interest. Looking at the displacement of the loudspeaker diaphragm it can be seen that the cut-off frequency for control is at 140 Hz. The behavior below the cut-off frequency when the excursion limit of the loudspeaker diaphragm has been reached looks a lot like the result seen in Figure 3.35 for the "Normal regeneration" test condition. Comparing the frequency response magnitude of the two test conditions in Figure A.6 and A.4 it can be seen that the spectrum is very similar, but the max levels are a bit different.

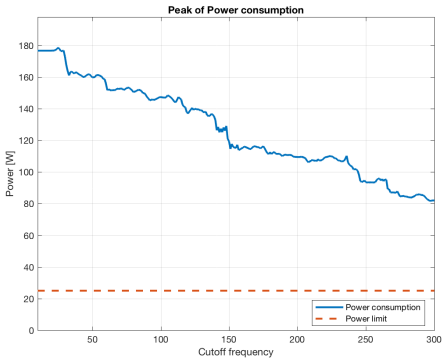

(a) Consumed power over frequency.

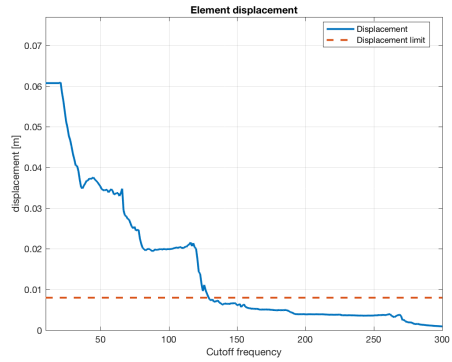

(b) Element displacement over frequency.

Figure 3.36: Results from study on consumed power and diaphragm displacement, New regeneration test condition.

4

Results

Here the results from the different parts of the project are presented. First results from the Chalmers rig were only offline control was implemented. Then results from the Volvo rig for both offline and online control.

4.1 Rig at Chalmers

The bandwidth to be controlled was between 20 Hz to 500 Hz for the offline controller at Chalmers. The reduction results are measured at the error microphone. All results shown in this section are presented without absolute values.

4.1.1 Results from offline control

Figure 4.1a shows the effect of the duct being heavily damped. Good and even reduction is obtained in the whole control interval with reduction between 20 dB to 30 dB apart from 150 Hz which is believed to come from a net grid interference. In Figure 4.1b the duct is lightly damped with the damping material removed from the duct resulting in stronger and narrower resonance peaks. Good reduction is obtained at the resonances but much lower at the nodes and thus the total reduction is less even than in the damped case.

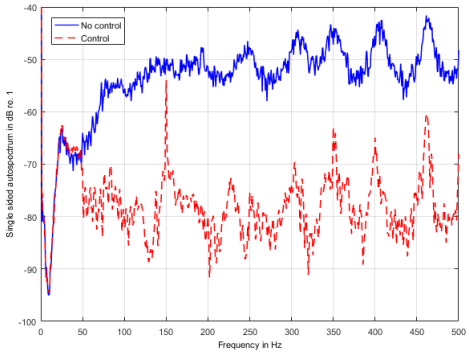

(a) Reduction in heavily damped duct. Control range 50-500 Hz.

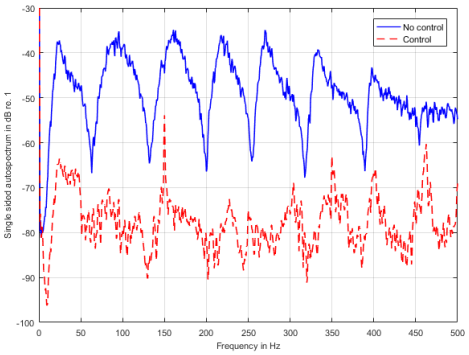

(b) Reduction in lightly damped duct 50-500 Hz

Figure 4.1: Reduction for heavily damped and lightly damped duct.

In a attempt to improve the result for wide-band control of the lightly damped duct the control frequency range was into two more narrow frequency ranges, 50 Hz to 150 Hz and 150 Hz to 500 Hz.

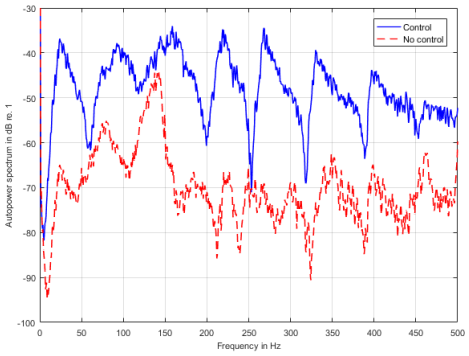

(a) Undamped control 50-500 Hz

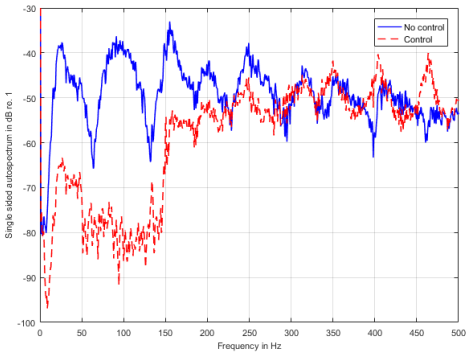

(b) Undamped control 50-150 Hz

Figure 4.2: White noise reduction at Chalmers duct

As seen in Figure 4.2 the narrowing of the control interval for the lightly damped duct didn't result in any improvement in reduction.

4.2 Rig at Volvo

In this section the results from the Volvo rig are presented. First results for offline control for the two different control loudspeaker positions with white noise as input. Next results from online control with white noise as source signal are presented for

different control filter filter lengths. Finally results from the online controller with the test conditions as source signal are presented.

4.2.1 Offline results

Figure 4.3 shows reduction recorded at the error microphone with white noise as source signal in offline mode. Figure 4.3a shows the reduction for the first speaker location and Figure 4.3b for the second. Recordings were done with the VXI workstation and Trigger Happy FFT analysing software.

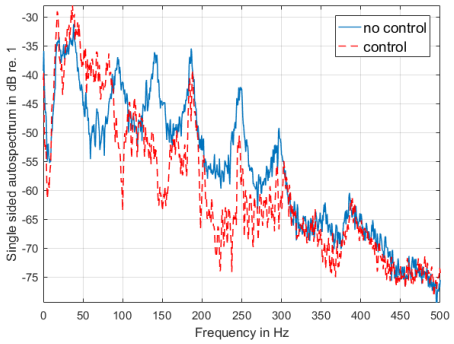

(a) Reduction from offline control with white noise as source. Control range 100-500Hz, first control loudspeaker location.

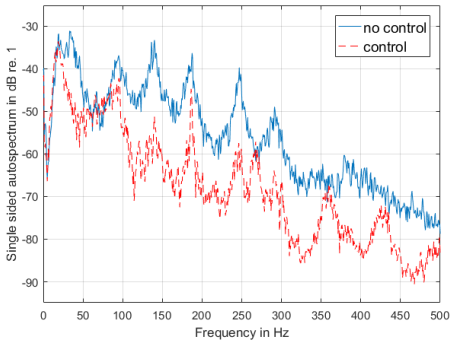

(b) Reduction from offline control with white noise as source. Control range 20-500Hz, second control loudspeaker location.

Figure 4.3: Reduction from offline control. Different control loudspeaker locations and different control range.

As seen in Figure 4.3 there is much less reduction in Figure 4.3a with the control loudspeaker in the first position, and there is some gain between 50 Hz and 100 Hz. In Figure 4.3b the loudspeaker is in it's final position and the control range has been extended down to 20Hz. Figure 4.3b shows how the reduction is greatly improved, showing the importance of the control loudspeaker location. After moving the control loudspeaker there was still gain between 50 Hz and 100 Hz with white noise as source signal, this was removed by lowering the control range down to 20 Hz.

4.2.2 Online results

In the development of the online controller several different filter lengths or number of filter coefficients were tested to find the optimum filter length. The filter needs to have sufficiently many coefficients to model the required response. Many filter coefficients will results in a slow convergence rate and few filter coefficients will result in less reduction.

In Figure 4.4 the obtained reduction recorded at the error microphone is shown for a controller with filter lengths of 256, 512 and 1024 coefficients respectively. In all cases the control filters are all zeros at the start and have been allowed to converge for the same amount of time for 1 min. Source signal is white noise and control range is 20 Hz to 300 Hz.

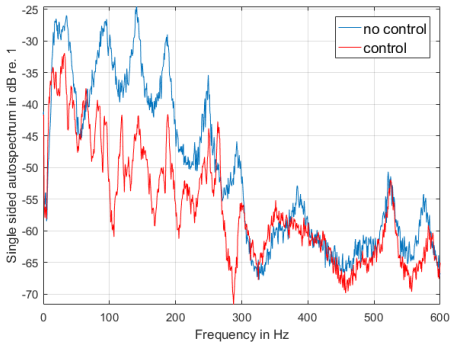

(a) Result 256 controller coefficients 20-300 Hz

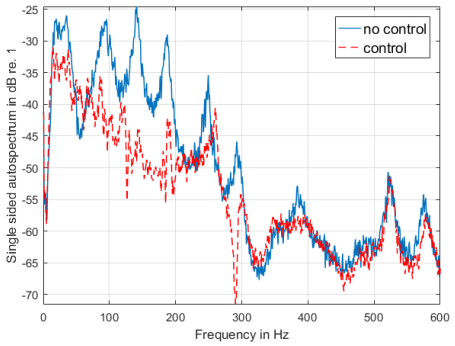

(b) Result 512 controller coefficients 20-300 Hz

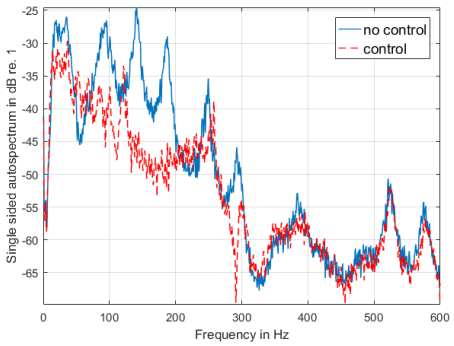

(c) Result 1024 controller coefficients 20-300 Hz

Figure 4.4: Reduction for different number of controller coefficients

Figure 4.4 shows the relationship between convergence rate and the number of filter coefficients. The control curves all have similar tendency but the one with 256 filter coefficients has the best reduction, therefore 256 filter coefficients were used in the online controller.

4.2.3 Test condition results

The final measurements for the online and offline controllers are now presented. Sound pressure levels recorded at the inlet mouth and acceleration recorded on the air intake(active side) and on the rig(passive side). All plots show reduction in dB for both sound pressure levels and acceleration levels. All measurements were done recording time series in Head Acoustics, Squadriga, analysis and plots were done in

Head Acoustics, Artemis Suite. The control range in is 100 Hz to 350 Hz. The lower limit for the controller was raised up to 100 Hz to protect the control loudspeaker. The gain at low frequencies observed in the offline control for white noise where not experienced in the online controller for the test conditions. The only gain observed in test condition measurements where for the "Compressor" in offline mode. The resolution of the y axis in the figures is the same for all SPL plots and same for all acceleration level plots, 10 dB for SPL plots and 5 dB for acceleration levels.

In Figure 4.5 the structure borne reduction results for the "Butterfly valve off" test conditions are shown. Figure 4.5a shows the active side measured with a accelerometer on the air intake and Figure 4.5b shows the passive side with the accelerometer on the alumimium rig.

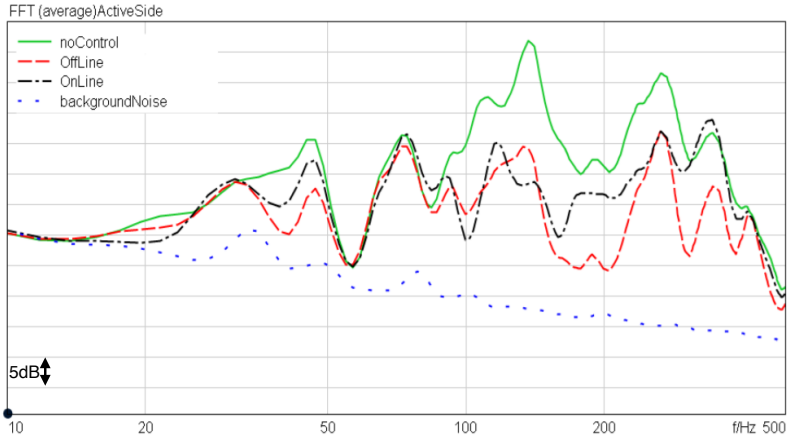

(a) Acceleration active side

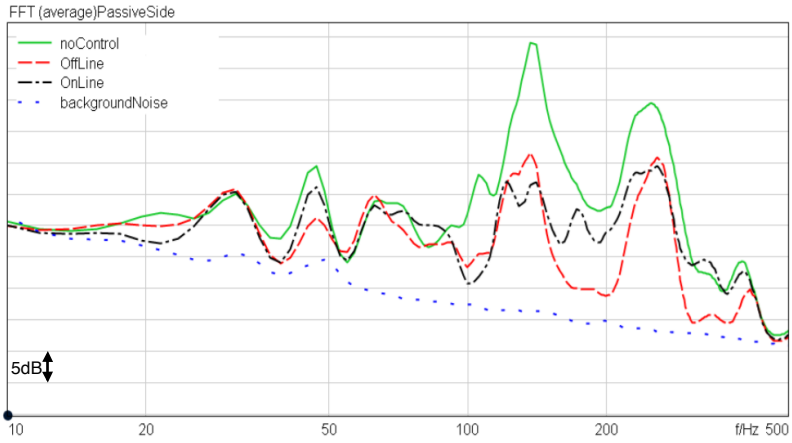

(b) Acceleration passive side

Figure 4.5: Butterfly valve off test condition results

The offline reduction on the active side is consistent in the control interval with reduction between 10 dB to 15 dB acceleration level. The reduction for the online controller is similar to the reduction for the offline controller at the resonances but less at the node at 200 Hz. Comparing the curves for no control in Figures 4.5a and

4.5b it can be seen how the rubber bushings reduce parts of the response although not much reduction is obtained at the resonances at 150 Hz and 250 Hz. At theses resonances is where the active control has the most reduction, around 15 dB in acceleration level. In Figure 4.6 the air borne reduction results for the "Butterfly valve off" test conditions are shown measured at the inlet mouth.

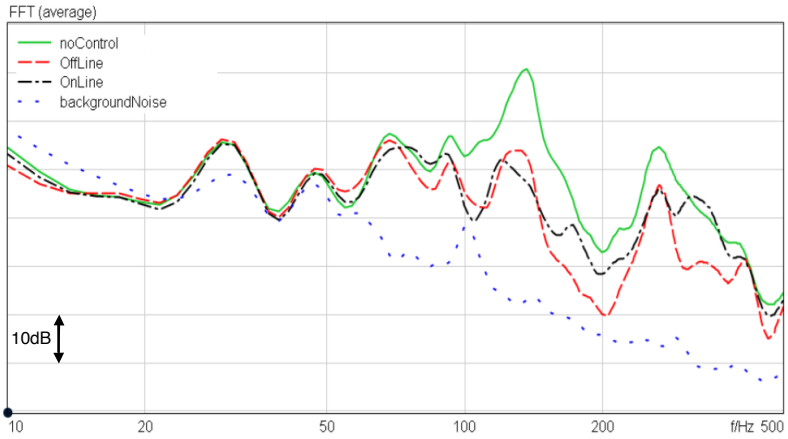

Figure 4.6: Sound pressure level at inlet mouth for "Butterfly off".

As seen in Figures 4.5 and 4.6 for "Butterfly valve off" the peak around 150 Hz is dominating and this is were most reduction is achieved. The online and offline controller results are mostly similar, as in the acceleration results the offline controller results have more reduction in the nodes than the online controller results. Obtained reduction levels are up to around 15 dB SPL. In Figure 4.7 the structure borne reduction results for the "Butterfly on" test condition are shown.

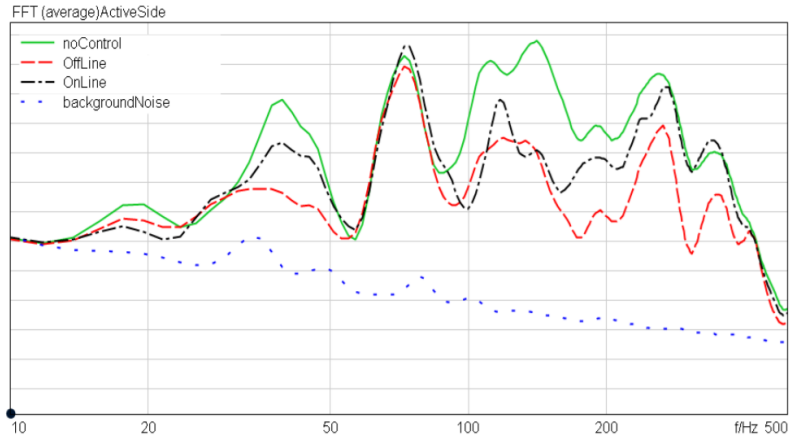

(a) Acceleration active side

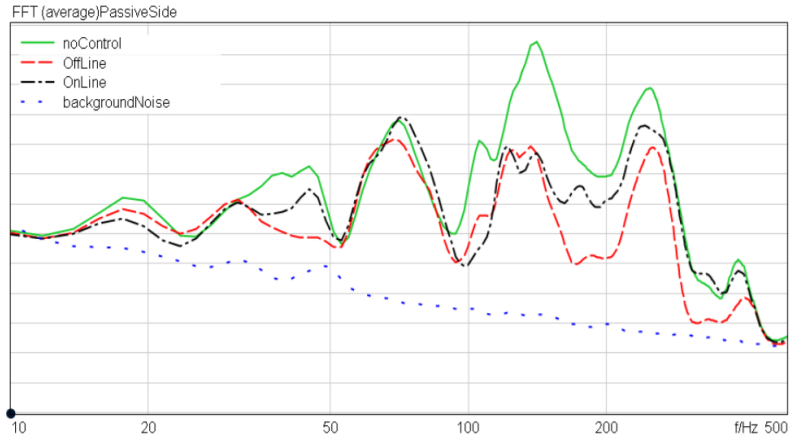

(b) Acceleration passive side

Figure 4.7: "Butterfly valve on" acceleration level results

In Figure 4.8 the air borne reduction results for the "Butterfly valve on" test conditions are shown measured at the inlet mouth.

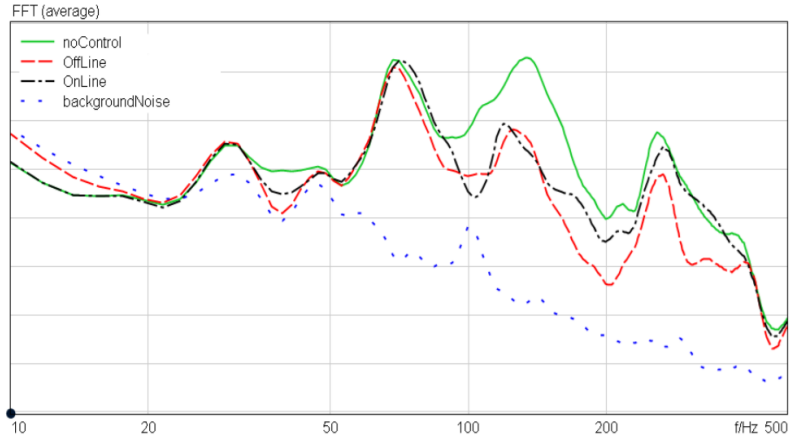

Figure 4.8: Sound pressure level at inlet mouth for "Butterfly valve on".

A clear difference between "Butterfly valve on" and "Butterfly valve off", in Figures 4.7, 4.8 and 4.5, 4.6 respectively is that in the "Butterfly valve on", a peak around 70 Hz is added to the spectrum. This is unfortunately outside the control range of 100 Hz to 350 Hz and thus not reduced. As in "Butterfly valve off" the peak at 150 Hz is dominant.

In the "Butterfly valve on" results the reduction in SPL is slightly less than for the "Butterfly valve off" results. Offline control is again slightly better than online, with similar reduction at the first peak at 150 Hz and less at the second peak at 250 Hz, offline control also has more reduction in the node between the peaks. In Figure 4.9 the structure borne reduction results for the "Compressor" test condition are shown.

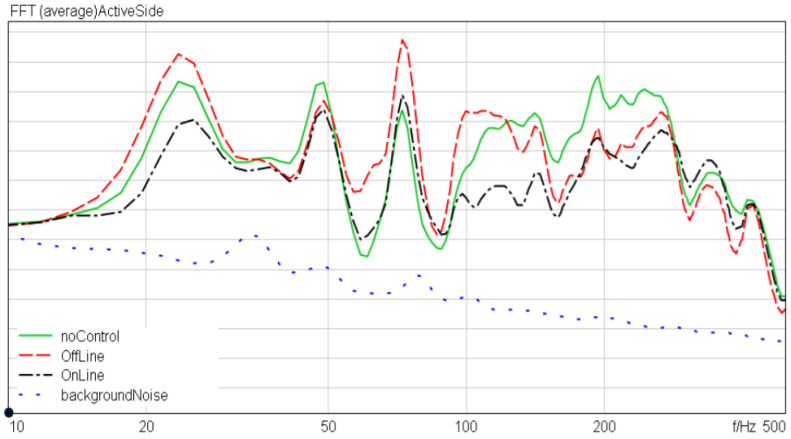

(a) Acceleration active side

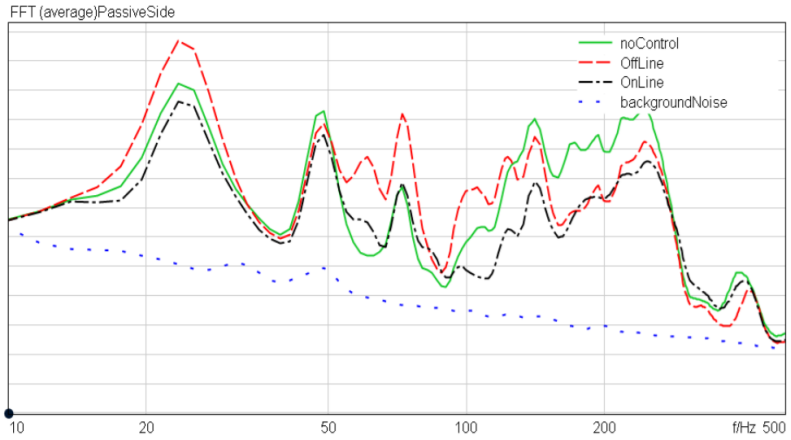

(b) Acceleration passive side

Figure 4.9: "Compressor" acceleration levels results

In Figure 4.10 the airborne reduction results for the "Compressor" are shown.

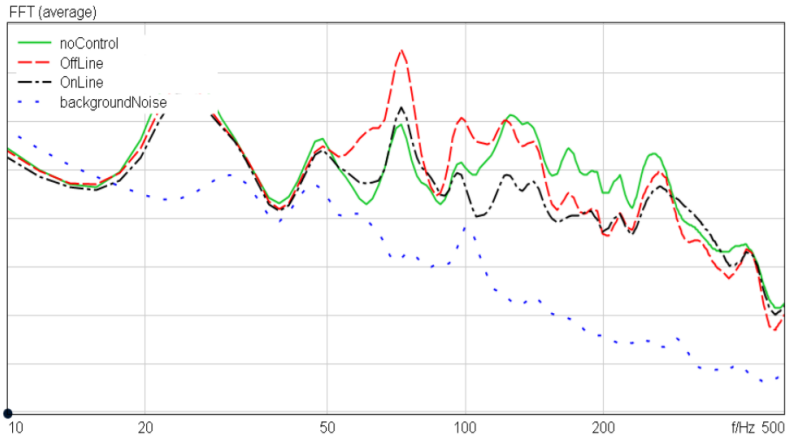

Figure 4.10: "Compressor" sound pressure level at inlet mouth.

Interesting to note in Figures 4.9 and 4.10 is that online is in general better both for acceleration levels and sound pressure levels. Offline has some gain outside the control interval, specifically at 30 Hz and 70 Hz and doesn't obtain reduction until after 150 Hz. After 150 Hz offline and online control are similar. Online control has hardly any gain and has reduction between 10 dB and 15 dB. What makes the "Compressor" test condition unique is that it is the test condition with most of it's energy at lower frequency than the other test conditions, around 30 Hz. The fixed characteristics off the offline controller obviously don't work well on this signal while the online controller has good results.

In the following the results from the regeneration test conditions are presented. First the "No regeneration" test condition which is without regeneration but otherwise has the same conditions as the regeneration conditions and serves as reference. Then the two regeneration test conditions, "New regeneration" and "Normal regeneration" are presented. The regeneration test conditions remind the "Butterfly on" test conditions, probably because the regeneration process also uses the butterfly valve. In Figure 4.11 the "No regeneration" structure born reduction results are shown.

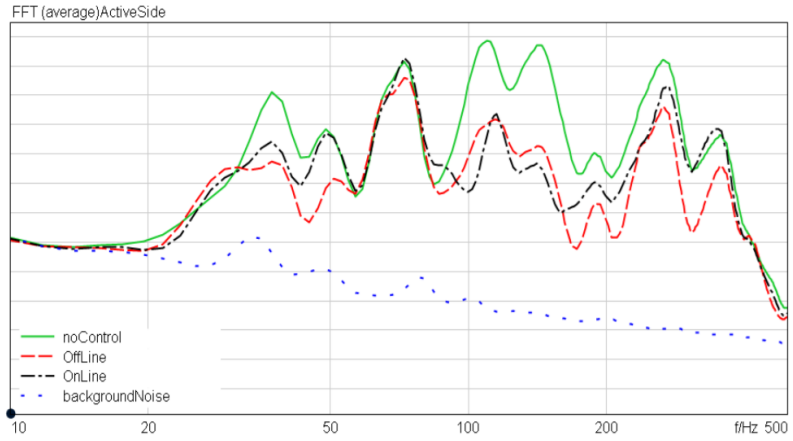

(a) Acceleration active side

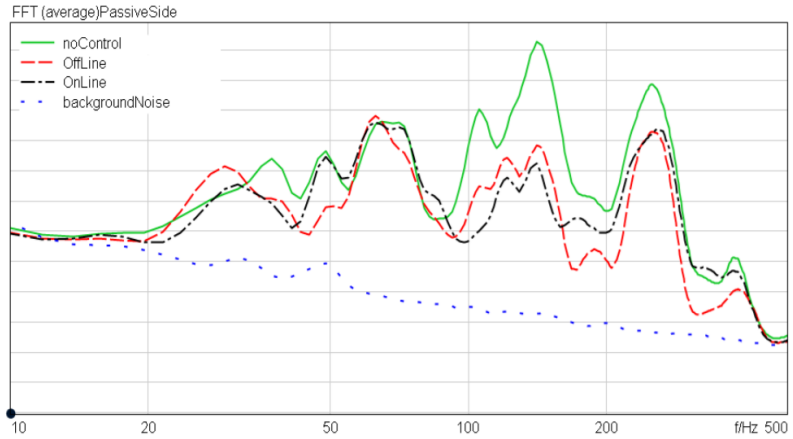

(b) Acceleration passive side

Figure 4.11: "No regeneration" acceleration levels results

Looking at Figures 4.11a and 4.11b it can be seen how active and passive control can work well together. The rubber bushings have reduced the peak just above 100 Hz leaving two peaks at 150 Hz and 250 Hz who are in the operating range of the active control and are significantly reduced by the active control. In Figure 4.12 the airborne reduction results for the "No regeneration" are shown.

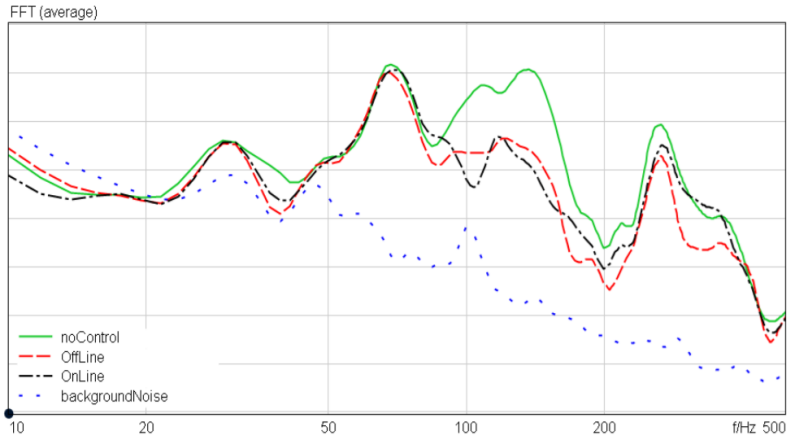

Figure 4.12: "No regeneration" sound pressure level at inlet mouth.

In Figure 4.12 showing the SPL it can be seen how the spectrum has a steep decline between 150 Hz to 200 Hz, at this frequency range control is reduced. This shows the behavior of the controller, reducing where the energy is highest and obtaining better reduction in regions where reference signal is flat in spectrum.The "New regeneration" structure borne reduction results are shown in Figure 4.13.

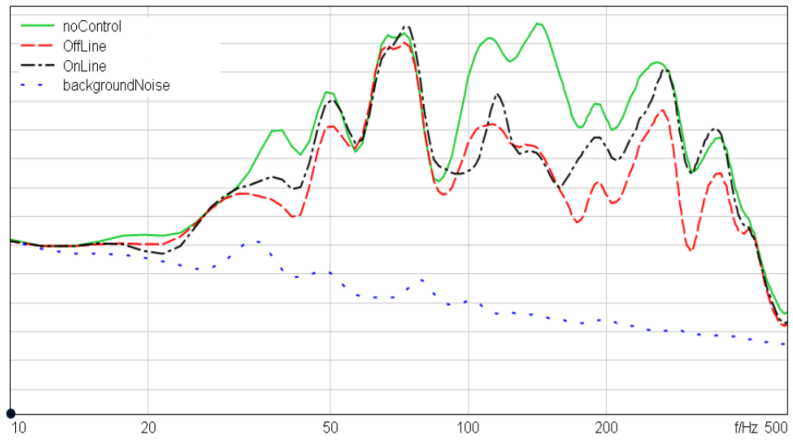

(a) Acceleration active side

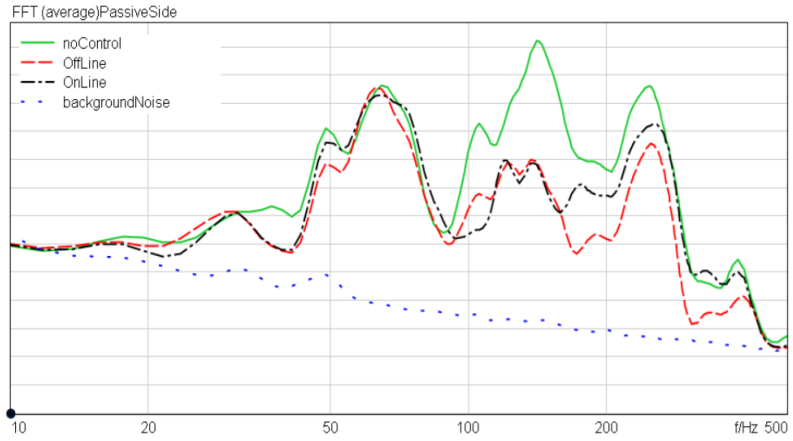

(b) Acceleration passive side

Figure 4.13: "New regeneration" acceleration levels results

The "New regeneration" air borne reduction results are shown in Figure 4.14.

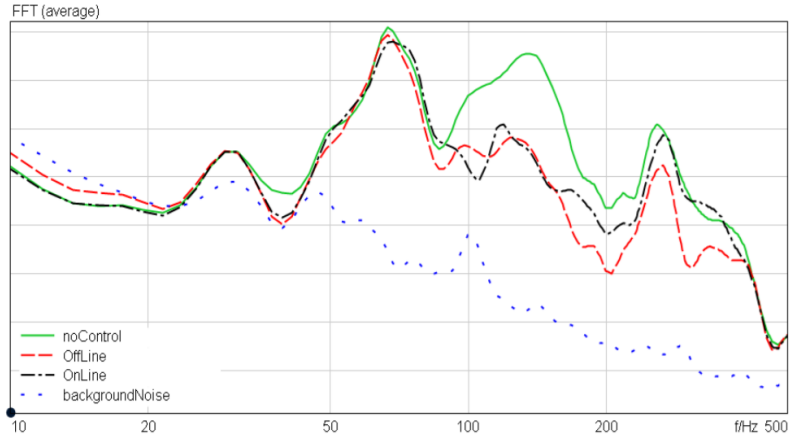

Figure 4.14: "New regeneration" sound pressure level at inlet mouth.

The "New regeneration" results in Figure 4.13 show peaks in the spectrum at 70 Hz and 150 Hz. Around 15 dB reduction is obtained for the peak at 150 Hz in both offline and online control. Offline is as before better at the 250 Hz peak. A difference between "New regeneration" in Figure 4.14 and "No regeneration" in Figure 4.12 is that the slope between 150 Hz to 200 Hz is not as steep in "New regeneration" as in "No regeneration" and thus better reduction is obtained in this region. In Figure 4.15 the normal regeneration test condition are shown.

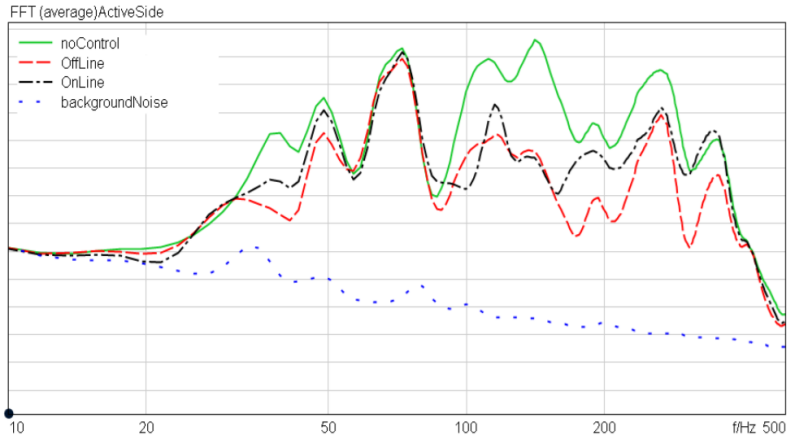

(a) Acceleration active side

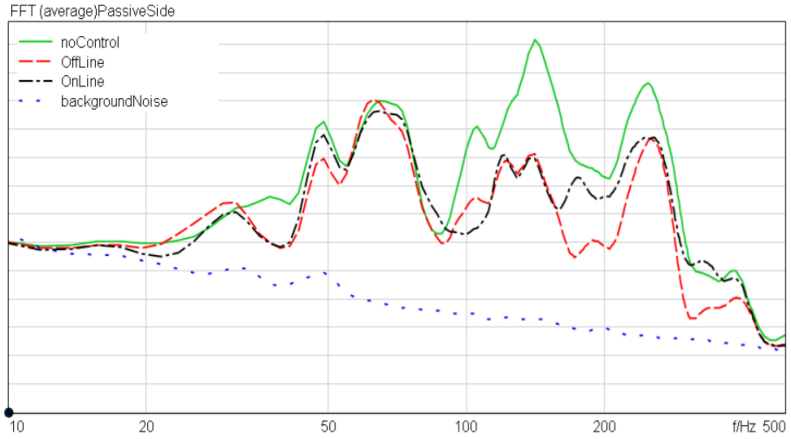

(b) Acceleration passive side

Figure 4.15: Normal regeneration test condition results

The "Normal regeneration" air borne reduction results are shown in Figure 4.16.

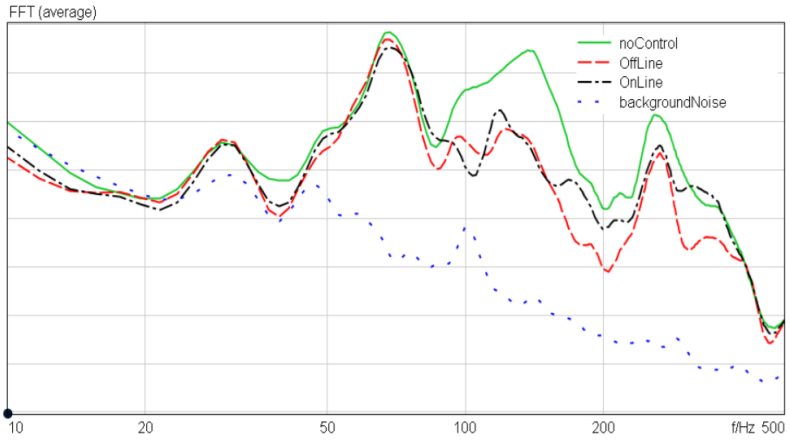

Figure 4.16: "Normal regeneration" sound pressure level at inlet mouth.

The "Normal regeneration" results are similar to the "New regeneration" and "No regeneration" ones. In the range between 100 Hz to 200 Hz they obtain similar reduction values. Observable difference is that for the peak at 250 Hz in the "Normal regeneration" the online controller obtains the same results as the offline controller

Interesting to note is that in all acceleration level results apart from the compressor there is some reduction below the control range between 30 Hz to 50 Hz. Although at these frequencies the response is quite low and just above the background noise.

5

Discussion

The project started out with an initial preparation phase at Chalmers were offine control was implemented on a small test-rig. The results from offline control for white noise at Chalmers, seen in Figure 4.1, show that it was more difficult for the controller to obtain an even reduction in the control interval 50 Hz to 500 Hz when the damping in the duct was low, especially in between resonances. This is because the contribution of many modes in between the resonances are causing the phase to move more rapidly then at resonances where the response is mostly contributed from one mode [4].

After the proposed offline controller had been tested at the test-rig at Chalmers the same controller was going to be implemented on a real truck air intake system from Volvo. The effect of finding a good control loudspeaker location proved to be a very important factor in the implementation as can be observed in Figure 4.3. At the initial control loudspeaker location the reduction on the air intake is not optimal, see Figure 4.3a. The reduction obtained with the control loud speaker in its optimized location can be seen in Figure 4.3b. The reduction levels obtained using stationary signals now remind of the reduction obtained at Chalmers test-rig seen in Figure 4.1. Moving the control loudspeaker to its optimal location reduced the acoustic distance to the reference microphone and therefore the delay in primary path.

The movement of the control loudspeaker decreased the delay for the system to react in time and resulted in a non causal system. The control system was made causal again by changing the analog anti aliasing and reconstruction filters to less steep filters with less delay. After these changes the condition $l_i/c \geq \delta_E$ is just barely fulfilled with one sample difference in delay in the primary path and secondary path. Despite this it is clear that the final position of the control loudspeaker greatly improves the obtained reduction.

With a delay difference of one sample in the final setup between the primary and secondary path at room temperature(20 °C), 14 and 13 samples respectively. Considering possible temperature variances in the system the question is if one sample difference is enough to implement a stable control system. The temperature that would be needed to reduce the delay in the primary path of one sample so that the delay in primary path would be equal to the delay in the secondary path can be

estimated with the following equation for the temperature dependency of the speed of sound in air: $c_{air} \approx 20.05\sqrt{273.2 + t}$, were t is the temperature in degrees Celsius [15]. The temperature increase needed to elevate the speed of sound so that the acoustic delay in the primary path would go down to be 13 samples long would need to be approximately 58 °C. Temperatures higher than that might cause violations of the causality constraint. In this project the actual temperature variances in the air intake have not been studied. All measurements were done at room temperature. It remains as future work to investigate the actual temperature variances in the air intake system.

To compensate for the secondary path the FxLMS filters the reference signal to the controller with a estimate of the secondary path, $\hat{C}(j\omega)$ which results in the controller response $-P(j\omega)/C(j\omega)$. The inverse frequency response function $1/C(j\omega)$ is a compensation for the actual secondary path frequency response function, being a part of the physical system. The chosen control interval of the controller will set the range of this compensation. If the frequency response function of the secondary path has high magnitudes at low frequencies, the control interval can be extended down in frequency to avoid gain problems outside the control interval. The final control interval of the controller was chosen to 100 Hz to 300 Hz. The upper limit being the cut off for plane waves at 380 hertz. Also the loss of energy in the test conditions above 300 Hz was considered when determining the upper cut off frequency so 300Hz was chosen. When choosing the lower limit of the controller the physical limitations of the control loudspeaker have to be accounted for. Since the displacement and power consumption of the control loudspeaker increase with lower frequencies, as discussed in Section 3.4, a balance between the lower frequency control interval limit and secondary path compensation must be considered. The lower limit of the control interval was chosen to 100 Hz partly since this is where the obtained magnitude of the frequency response function for $P(j\omega)$ provides acoustic information of the duct to the controller and partly due to the control loudspeaker limitations. The lower limit set to 100 Hz resulted in no gain in the test conditions apart from the "Compressor" test condition in offline mode.

After the initial offline controller was implemented and tested on the air intake system at Volvo a online controller was designed. For a steady state disturbance signal, speed of the online controller is not a big problem but as soon as the signal is non stationary convergence speed is a limiting factor. This is due to the fact that the filter coefficients adapt to the frequency content in the block of samples acquired by the controller. For a filter length of 256 coefficients the time it takes for the controller to fill a block of samples is 50 ms For a controller with 512 filter coefficients it will take the controller 100 ms to fill a block of data for the same sample time of 5120 Hz. In Figure 4.4c it can be seen that the controller is still converging after several minutes of training. For a non stationary signal the convergence time of the control filter has to keep up with the rate of change of frequency content in the input signal. The control filters optimal solution is then moving around continuously.

In an attempt to increase the obtained reduction of the online controller averaging the control filter coefficients was tested. Using averaging in online control proved to be more problematic since the control filter has to have converged before averaging takes place otherwise it will results in much longer convergence time. If the reference signal is non stationary the control filter coefficients are updated continuously according to the changes in the reference signal and estimation of the primary path. No improvement in reduction was obtained averaging the control filter coefficients, therefore time averaging was not implemented in the final controller.

The influence of the test conditions frequency response magnitude on the optimal solution as discussed in 2.4 was also investigated, seen in section B when stationary white noise and the non-stationary test conditions respectively are used to estimate the primary path at the Volvo test-rig. The energy per hertz in white noise is constant, giving a good primary path estimation for all frequencies within the control interval (100 Hz to 350 Hz) given that the estimation has converged, see Figures B.1b, B.2a, B.4a, B.5a and B.6a.

In the test condition results seen in section 4.2.3 it can be seen that both offline and online are reducing the vibration levels through the bushing of the inlet pipe into the cabin effectively. It can be seen that all of the controllers are aiming to reduce the higher energy vibration levels over the smaller energy vibrations. This reflects the importance of the energy content per hertz in the reference signal for the controller. The magnitude of all test conditions is higher at 150 Hz then at 250 Hz. This is the frequency range where the controller is able the reduce the wave-front in the duct the most.

6

Conclusion and future work

It can be concluded that implementing active noise control on the air intake system was technically possible. Both airborne sound recorded at the inlet mouth and structure borne vibrations measured on the test rig where successfully reduced.

It was demonstrated that using an ergodic white noise reference signal gave a better reduction of the sound pressure level in the inlet system then when the non stationary signal was used. The results show that the offline controller using a ergodic training signal has in general slightly better reduction results than the online controller. While the offline controller is probably not feasible to implement in a real truck due to changes in the transfer functions as a result of temperature changes, this leads to the idea that a hybrid between offline and online could be a good solution. This could be done by estimating the transfer functions $P(j\omega)$ and $C(j\omega)$ and then calculating a controller, $H(j\omega)$ with the offline method. The problem would then be to get a good estimation for $P(j\omega)$. The results in estimation plots show that $P(j\omega)$ gets a good estimation in the lower range of the control interval. By narrowing the interval down to were $P(j\omega)$ gets a good estimation, this could be done. The results also show that in online there is good reduction in the lower frequency range of the control interval. This is due to the fact that this is where the test conditions have most power and thus the estimation of $P(j\omega)$ will be best in this range. If a pure online controller is chosen for future work the control interval should perhaps be narrowed down to the range were $P(j\omega)$ gets a good estimation with the test conditions as source.

The study on the control loudspeaker shows that the loudspeaker is not able to operate on the sound pressure levels of the on-situ test conditions in the desired frequency band. Future work should include a study of a new type of control loudspeaker that can handle the true sound pressure levels of a on-situ truck.

Bibliography

[1] S. F. Amundsen Astrid H., "Hours of service regulations and the risk of fatigue-and sleep-related road accidents," *TØI*, 2003.

[2] A. Genell, *Phd thesis;Perception of sound and vibration in heavy trucks*. Chalmers University, 2008.

[3] C. Hansen, S. Snyder, X. Qiu, L. Brooks, and D. Moreau, *Active Control of Noise and Vibration, Second Edition*. CRC Press, 2012.

[4] P. Nelson and S. Elliott, *Active Control of sound*. Academic press, 1992.

[5] I. L. . L. L. Beranek, *Noise and vibration control engineering,second edition*. John Wiley & Sons, 2006.

[6] W. Kropp, *Active noise control lecture notes*. Chalmers University, 2016.

[7] B. Widrow and S. D.Stearns, *Adaptive signal processing*. Prentice-Hall, 1985.

[8] T. McKelvey, *Applied signal processing lecture notes*. Chalmers University, 2014.

[9] P. S. R. Diniz, *Adaptive Filtering*. Springer, 2013.

[10] Y. L. Mingsian R. Bai and J. Lai, "Reduction of electronic delay in active noise control systems— a multirate signal processing approach," *The Journal of the Acoustical Society of America*, 2002.

[11] S. L.Miller, *Probability and random processes,second edition*. Academic press, 2014.

[12] L. L. . T. J. Mellow, *Acoustics, Sound Fields and Transducers*. Academic Press, 2012.

[13] M. Rossing and Wheeler, *The science of sound,third edition*. Addison Wesley, 2002.

[14] M. Kleiner, *Acoustics and audio technology,third edition.* J.Ross Publishing, 2012.

[15] V. E. Tor, *Building Acoustics.* Taylor & Francis, 2008.

A

Test Conditions

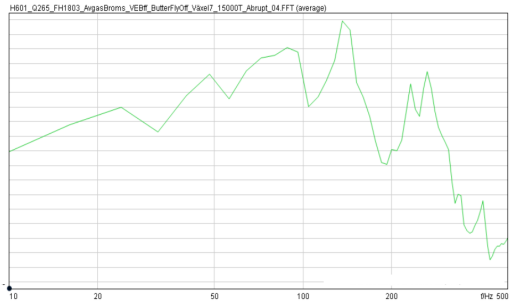

(a) Frequency magnitude

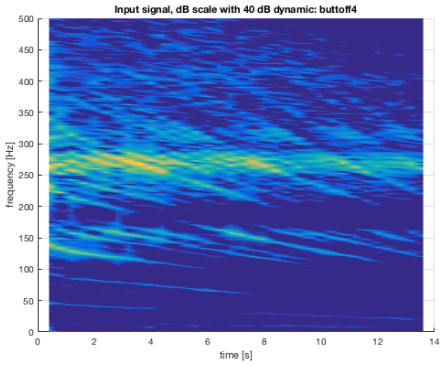

(b) Spectrogram

Figure A.1: Butterfly valve off test condition

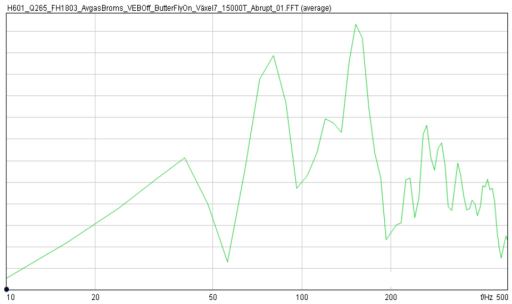

(a) Frequency magnitude

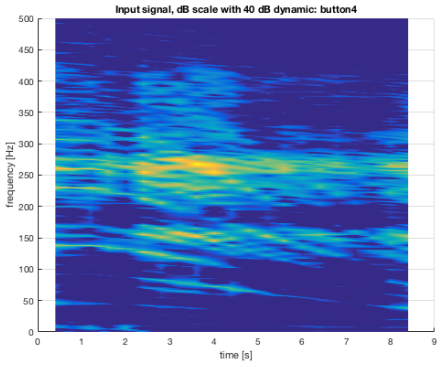

(b) Spectrogram

Figure A.2: Butterfly valve on test condition

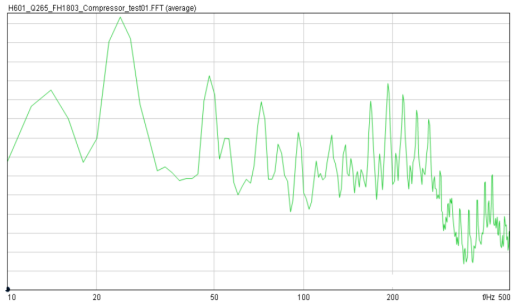

(a) Frequency magnitude

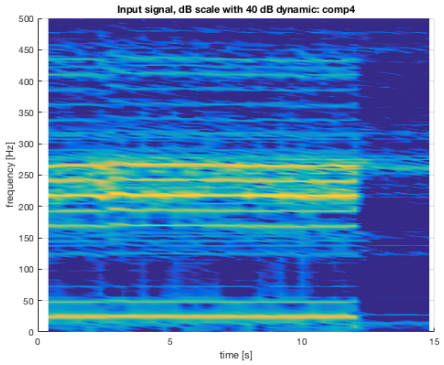

(b) Spectrogram

Figure A.3: Compressor test condition

(a) Frequency magnitude

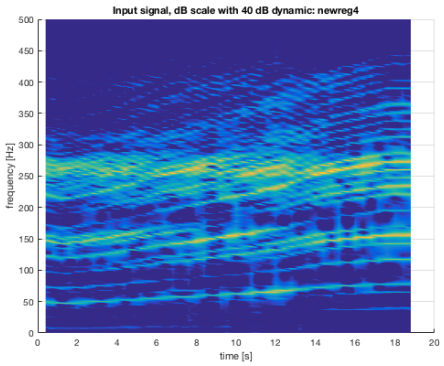

(b) Spectrogram

Figure A.4: New regeneration test condition

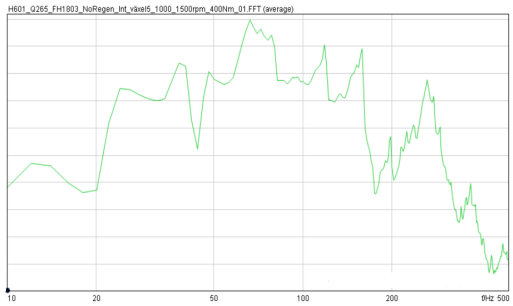

(a) Frequency magnitude

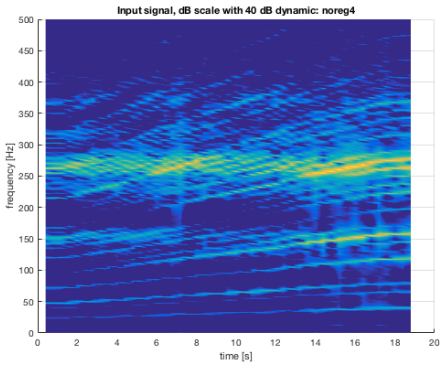

(b) Spectrogram

Figure A.5: No regeneration test condition

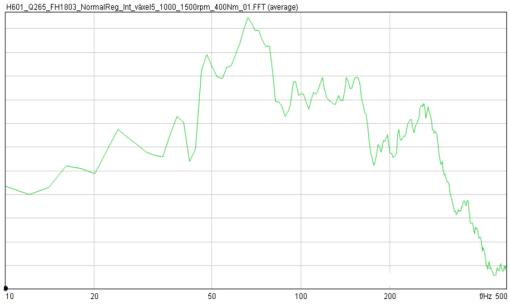

(a) Frequency magnitude

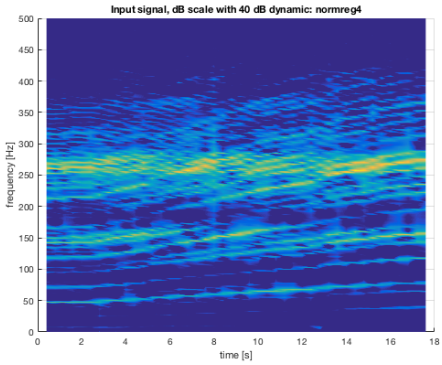

(b) Spectrogram

Figure A.6: Normal regeneration test condition

B

Estimation of primary path transfer function with different source signals

The following plots show estimation of primary path with test conditions and white noise done in Simulink. Estimation with test conditions was done over the time duration of the respective test condition length and each respective estimation with white noise with the same time length.

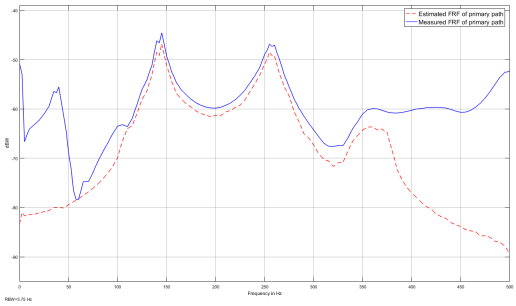

(a) Estimation, white noise.

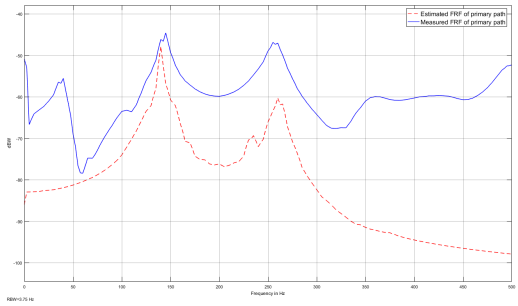

(b) Estimation, Butterfly valve off.

Figure B.1: Estimation of primary path with white noise(a), and Butterfly valve off(b) as source signals. Duration 22.6s.

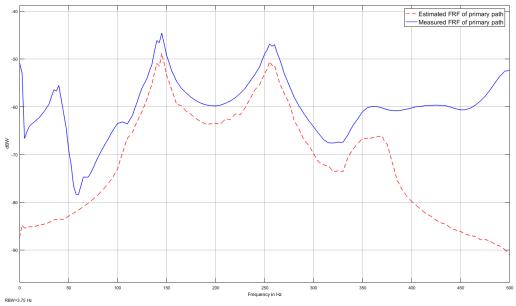

(a) Estimation, white noise.

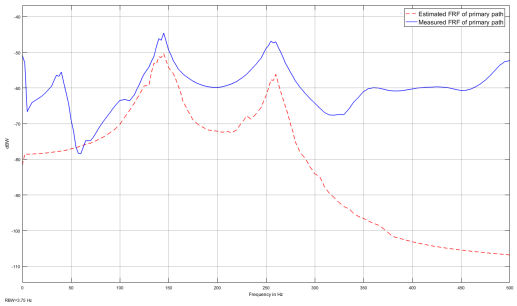

(b) Estimation, Butterfly valve on.

Figure B.2: Estimation of primary path with white noise(a), and Butterfly valve on(b) as source signals. Duration 13.8s.

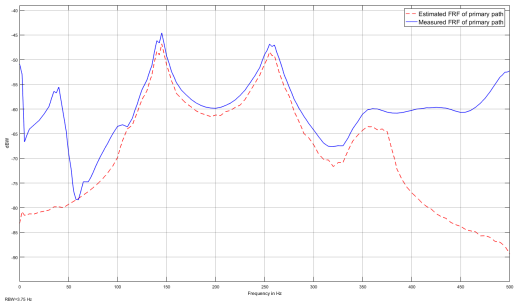

(a) Estimation white noise

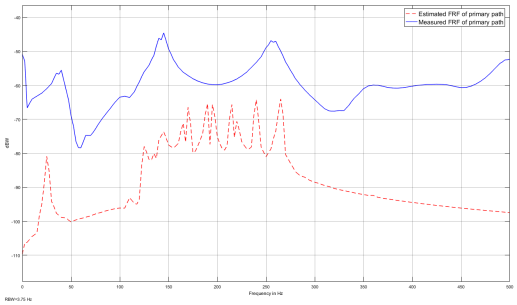

(b) Estimation compressor

Figure B.3: Estimation of primary path with white noise(a), and Compressor(b) as source signals. Duration 23.1s.

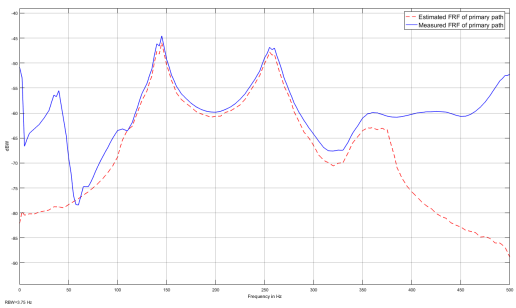

(a) Estimation white noise

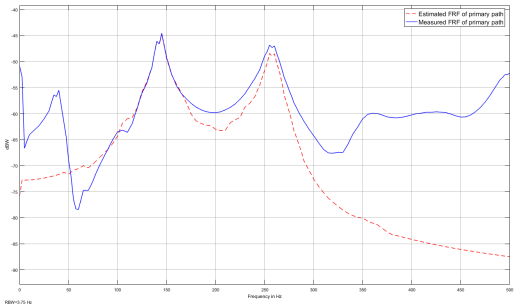

(b) Estimation, New regeneration on.

Figure B.4: Estimation of primary path with white noise(a), and New regeneration(b) as source signals. Duration 28.9s.

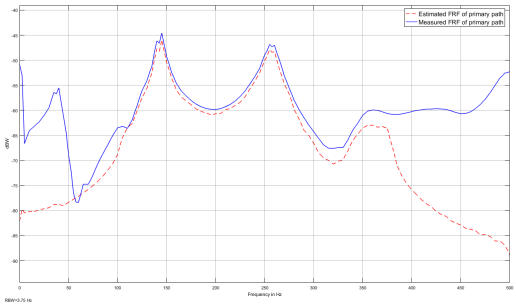

(a) Estimation white noise

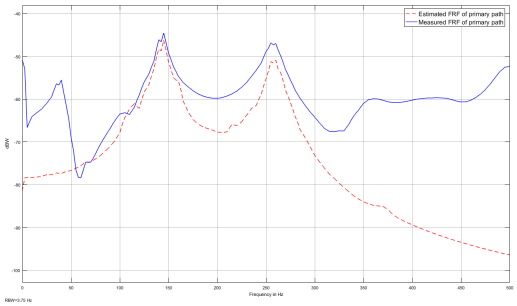

(b) Estimation, No regeneration on.

Figure B.5: Estimation of primary path with white noise(a), and No regeneration(b) as source signals. Duration 28.5s.

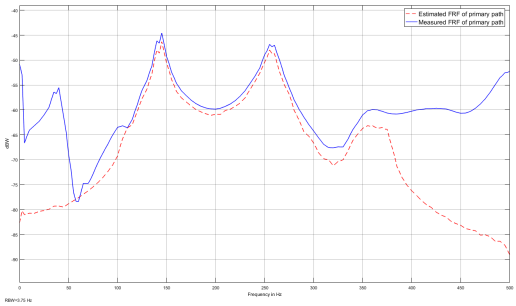

(a) Estimation white noise

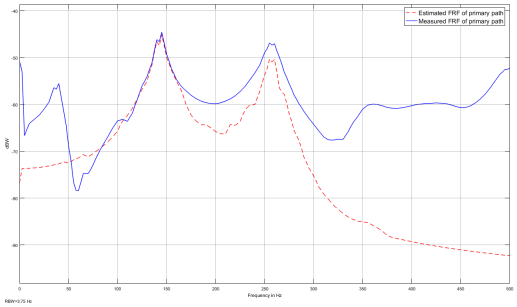

(b) Estimation, Normal regeneration on.

Figure B.6: Estimation of primary path with white noise(a), and Normal regeneration(b) as source signals. Duration 26.3s.

C

Equipment

C.1 Equipment list at Chalmers

- NAD 3020, Integrated Stereo Amplifier
- KEMO,Analog filter bank, 48dB/octave
- VXI, Data Acquisition Station
- HP, Two PC-Computers
- Error microphone
- Reference microphone
- G.R.A.S, Microphone pre-amplifier
- Trigger Happy, custom sub-software called in MATLAB.
- Cables
- Two closed loudspeakers
- Pvc duct
- dSpace, DSP
- dspace, controller board, ds1103

C.2 Equipment list at Volvo

- KEMO,Analog filter 48dB/octave
- KEMO,Analog filter 24dB/octave
- Custom,Analog filter 12dB/octave
- Brüel & Kjær probe microphone, 4182,1510141
- Brüel & Kjær probe microphone, 4182,1818518
- Svantek, Svan 959 measurement device
- G.R.A.S microphone,26CA,228212
- G.R.A.S microphone, 46AO,MIK29460
- Brüel & Kjær accelerometer,4374, 12206
- Brüel & Kjær accelerometer, 4507B,2307502
- Brüel & Kjær accelerometer,4508B,2199128
- Brüel & Kjær charge to deltatron converter,2647
- B&W, subwoofer,CT SW10
- Microphone preamp, Brüel & Kjær, 47002
- Visaton KT100 25W speaker in custom enclosure.
- Air intake pipe from a Volvo truck mounted on a aluminium rig.
- VXI-Data Acquisition Station
- Two PC-Computers
- DSP, dSpace processor
- dspace ds1103 controller board
- dSpace,Software, Control Desk from dSpace
- Trigger Happy,Software , custom sub-software called in MATLAB.

- Matlab,Software
- Head Acoustics,Software, Artemis Suite
- Head Acoustics, Squadriga Mobile Recording and Playback System.
- Labgruppen,Integrated Stereo Amplifier,Lab 300
- Preamp
- Cables
- Audiomatica acquisition system with Clio 10 software

D

Data sheet: Visaton KT 100 V - 4 Ohm

KT 100 V - 4 Ohm

Art. No. 9070

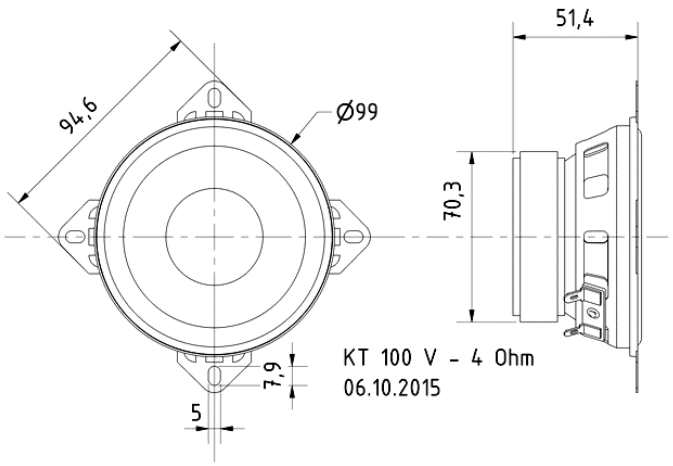

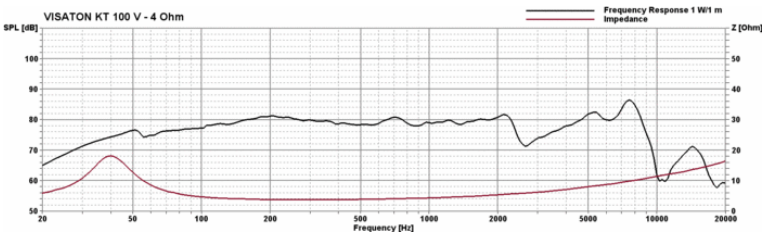

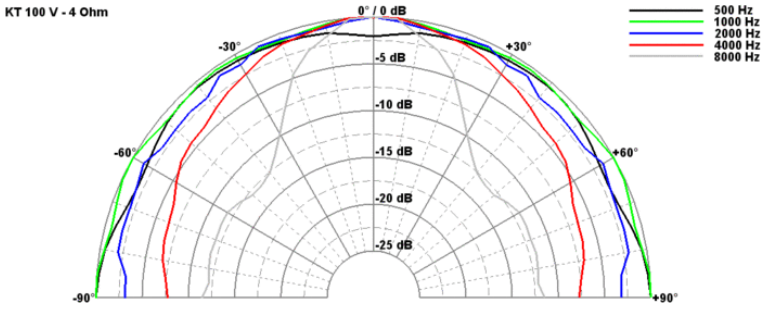

Technische Daten / **Technical data**

Nennbelastbarkeit Rated power	25 W
Musikbelastbarkeit Maximum power	40 W
Nennimpedanz Z Nominal impedance Z	4 Ohm
Übertragungsbereich Frequency response	32–9500 Hz
Mittlerer Schalldruckpegel Mean sound pressure level	80 dB (1 W/1 m)
Resonanzfrequenz fs Resonance frequency fs	37 Hz
Obere Polplattenhöhe Height of front pole-plate	3 mm
Schwingspulendurchmesser Voice coil diameter	25 mm
Wickelhöhe Height of winding	7 mm
Schallwandöffnung Cutout diameter	92 mm
Gewicht netto Net weight	0,466 kg
Gleichstromwiderstand Rdc D.C. resistance Rdc	3,6 Ohm
Mechanischer Q-Faktor Qms Mechanical Q factor Qms	2,22
Elektrischer Q-Faktor Qes Electrical Q factor Qes	0,54
Gesamt-Q-Faktor Qts Total Q factor Qts	0,43
Äquivalentes Luftnachgiebigkeitsvolumen Vas Equivalent volume Vas	9,8 l
Effektive Membranfläche Sd Effective piston area Sd	54,1 cm²
Dynamische bewegte Masse Mms Dynamically moved mass Mms	7,5 g
Antriebsfaktor Bxl Force factor Bxl	3,43 Tm
Anschlüsse Connections	4,8 x 0,8 mm (+) 2,8 x 0,8 mm (–)

09.11.2015

VISATON GmbH • Ohligser Straße 29-31 • D-42781 Haan • Tel.: 02129/552-0 • Fax 02129/552-10 • E-Mail: visaton@visaton.com

E

Data sheet: Bowers & Wilkings CT SW10

Bowers & Wilkins

Custom Theatre
CT SW10

Listening is believing

Spectacular explosions and high-speed car crashes will never sound as gloriously punchy, life-like and rich in detail as they will from our Custom Theatre subwoofers. Powered by a separate SA1000 amplifier, the CT SW10 slots neatly into a home theatre cabinetry and uses a uniquely rigid mushroom diaphragm construction to deliver unparalleled bass effects. The CT SW10 is the entry point in the range, delivering powerful bass through a 10 inch paper/Kevlar® driver.

Technical Specifications

Technical features	**Long throw Paper/Kevlar® cone bass driver** **Magnetically atached grille**
Description	Closed box subwoofer
Drive units	1x Ø250mm (10 in) paper/Kevlar® bass unit
Frequency range	-6dB at 18Hz and 25/140Hz adjustable (EQ at A) (with SA1000 subwoofer amplifier)
Frequency response	±3dB 26Hz – 40/140Hz adjustable (EQ at A) (with SA1000 subwoofer amplifier)
Recommended amp power	1000W into 4 Ω on unclipped programme (SA1000 subwoofer amplifier)
Max. recommended cable impedance	0.1Ω
Dimensions	Height: 360mm (14.2 in) Width: 340mm (13.4 in) Depth: 260mm (10.3 in) Depth with grille: 290mm (11.4 in)
Net weight	15kg (33lb)
Finish	Cabinet: Black painted Grille: Black cloth